T.C.
YEDITEPE UNIVERSITY
INSTITUTE OF HEALTH SCIENCES
DEPARTMENT OF MEDICAL PHYSICS

IMAGE-BASED RED BONE MARROW BIODISTRIBUTION AND DOSIMETRY OF ^{177}Lu[Lu]-PSMA-617 IN PATIENTS WITH METASTATIC PROSTATE CANCER

MASTER THESIS

BERFU NACAR

İstanbul , 2022

T.C.
YEDITEPE UNIVERSITY
INSTITUTE OF HEALTH SCIENCES
DEPARTMENT OF MEDICAL PHYSICS

IMAGE-BASED RED BONE MARROW BIODISTRIBUTION AND DOSIMETRY OF ^{177}Lu[Lu]-PSMA-617 IN PATIENTS WITH METASTATIC PROSTATE CANCER

MASTER THESIS

BERFU NACAR

SUPERVISOR
Prof. Dr. Ş. İpek KARAASLAN

CO-ADVISOR
Postdoc. Dr. rer.nat. Seval BEYKAN

İstanbul , 2022

THESIS APPROVAL FORM

Institute : Yeditepe University Institute of Health Sciences

Programme : Medical Physics Master Program

Title of the Thesis : Image-based red bone marrow biodistribution and dosimetry of ^{177}Lu[Lu]-PSMA-617 in patients with metastatic prostate cancer

Owner of the Thesis : Berfu Nacar

Examination Date : 24.09.2022

This study have approved as a Master Thesis in regard to content and quality by the Jury.

	Title, Name-Surname (Institution)
Chair of the Jury: Supervisor:	Prof. Dr. Şerife İpek KARAASLAN Yeditepe University
Supervisor:	Postdoc. Seval BEYKAN Würzburg University
Member/Examiner:	Prof. Dr. Nalan Alan SELÇUK Yeditepe University
Member/Examiner:	Doç. Dr. Zuhal ER Istanbul Technical University
Member/Examiner:	Prof. Dr. Nesrin ALTINSOY Istanbul Technical University

APPROVAL

This thesis has been deemed by the jury in accordance with the relevant articles of Yeditepe University Graduate Education and Examinations Regulation and has been approved by Administrative Board of Institute with decision dated ..... and numbered .....

Prof. Dr. Bayram YILMAZ

Director of Institute of Health Sciences

DECLARATION

I hereby declare that this thesis is my own work, which rely on the best of my knowledge and belief, it contains no material previously published or written by another person nor material which has been accepted for the award of any other degree except where due acknowledgment has been made in the text.

24.09.2022

BERFU NACAR

ACKNOWLEDGEMENTS

I would like to thank my supervisor Prof. Dr. Ş. İpek KARAASLAN and co-advisor Postdoc. Dr. rer.nat. Seval BEYKAN

I am grateful to my mother Derya NACAR and my sister Gizem NACAR for always being there for me.

Additionally, I would also like to thank my teacher Dr. Türkay TOKLU and my colleague Levent ERTOKTAŞ who supported me.

TABLE OF CONTENTS

LIST OF TABLES

LIST OF FIGURES

ABBREVIATIONS

2D	Two dimensional
3D	Three dimensional
Ac	Actinium
Bq	Becquerel unit
Ci	Curie unit
Cps	Counts per second
CT	Computed Tomography
EMA	European Medicines Agency
FDA	Food and Drug Administration
Ga	Gallium
h	Hour
Hf	Hafnium
ICRP	International Commission on Radiological Protection
Lu	Lutetium
LV2-4	Lumbar vertebrae 2-4
MEGP	Medium Energy General Purpose
MIRD	Medical Internal Radiation Dosimetry
OSEM	Ordered Subset Expectation Maximization
PET	Positron Emission Tomography
PSMA	Prostate-Specific Membrane Antigen
SPECT	Single Photon Emission Computed Tomography
$T_{1/2}$	Half life of a radionuclide
TAC	Time-uptake curve
T_{eff}	Effective half life of a radionuclide
TIAC	Time integrated activity coefficient
T_{scan}	Scan time
WB	Whole body
α	Alpha
β	Beta
γ	Gamma

ABSTRACT

Nacar B. Image-based red bone marrow biodistribution and dosimetry of ^{177}Lu[Lu]-PSMA-617 in patients with metastatic prostate cancer. Yeditepe University Institute of Health Sciences, Department of Medical Physics, MSc Thesis, İstanbul

^{177}Lu[Lu]-PSMA-617 therapy applied in the nuclear medicine department is a very promising treatment for metastatic castration-resistant prostate cancer patients for treatment response, so it has become very popular recently. ^{177}Lu[Lu]-PSMA-617, which has recently received FDA and EMA approval, is not among the standardized nuclear medicine treatments; therefore, it is essential to apply patient-specific personalized dosimetry for this application. PSMA, an antigen with specific uptake property for prostate cancers, is combined with ^{177}Lu radionuclide and injected into patients. Because of the physical properties of the ^{177}Lu radionuclide, it is possible to perform ^{177}Lu[Lu]-PSMA-617 dosimetry by using nuclear medicine imaging techniques. As a result, the absorption dose values of the relevant organs and tumors can be calculated in order to determine how much damage is caused to the tumor and healthy organs as a result of the treatment applied. Calculation of the absorb dose value of the bone marrow, which is specified as the organ at risk in the treatment of ^{177}Lu[Lu]-PSMA-617, is an important criterion in documenting the reliability of the applied treatment and planning the subsequent ^{177}Lu[Lu]-PSMA-617 treatments. The main purpose of the applied dosimetry is to cause maximum damage to tumors while causing as little damage to healthy tissues as possible. Bone marrow dosimetry can be performed in two different ways: using blood measurements or nuclear medicine imaging techniques. There is no standardized or proven method in this regard. In this thesis, image-based dosimetry method was used for bone marrow dosimetry. The post-treatment bone marrow doses of patients with metastatic castration-resistant prostate cancer treated with ^{177}Lu[Lu]-PSMA-617 included in the thesis study were calculated using different scanning modes. These scanning modes were performed using multiple 3D images (scanning mode 1), multiple 2D images and one 3D image (scanning mode 2), and a single 3D image (scanning mode 1). Bone marrow absorb dose values obtained due to three different scanning modes were compared with each other and with previously published literature data. This is the first study to calculate and compare personalized bone marrow absorb dose values using 3 different scanning modes in patients treated with ^{177}Lu[Lu]-PSMA-617.

Key Words: Image based dosimetry, Bone marrow dosimetry, Lute

ÖZET

Nacar, B. Metastatik prostat kanseri hastalarında ^{177}Lu[Lu]-PSMA-617'nin görüntü bazlı kırmızı kemik iliği biyodağılımı ve dozimetrisi. Yeditepe Üniversitesi Sağlık Bilimleri Enstitüsü, Sağlık Fiziği ABD., Master Tezi

Nükleer tıp departmanında uygulanan ^{177}Lu[Lu]-PSMA-617 tedavisi, tedavi yanıtı değerlendirildiğinde metastatik kastrasyona dirençli prostat kanseri hastaları için oldukça umut verici bir tedavidi; bu sebeple son zamanlarda oldukça popüler hale gelmiştir. Yakın zaman önce FDA ve EMA onayı alan ^{177}Lu[Lu]-PSMA-617 standardize edilmiş nükleer tıp tedavileri arasında yer almamaktadır. Bu nedenle bu uygulama için hastaya özel kişiselleştirilmiş dozimetri uygulamak elzemdir. Prostat kanserlerine spesifik tutulum özelliği mevcut bir antijen olan PSMA, ^{177}Lu radyonükliti ile birleştirilerek hastalara enjekte edilir ve bu uygulama sonrasında ^{177}Lu radyonüklitinin fiziksel özellikleri sayesinde, nükleer tıp görüntüleme tekniklerinden yararlanıp ^{177}Lu[Lu]-PSMA-617 dozimetrisi yapmak mümkündür. Bu sayede uygulanan tedavi sonucunda tümörlü ve sağlıklı organlarda ne kadar hasara yol açıldığını tespit edebilmek için ilgili organların ve tümörlerin absorbe doz değerleri hesaplanabilir. ^{177}Lu[Lu]-PSMA-617 tedavisinde kritik organ olarak sınıflandırılan kemik iliğinin absorbe doz değerinin hesaplanması uygulanan tedavinin güvenilir olup olmadığını belgelemede ve devamında uygulanacak ^{177}Lu[Lu]-PSMA-617 tedavilerinin planlanmasında önemli bir kriterdir. Uygulanan dozimetrinin ana amacı tümörlü dokulara maksimum hasarı verip sağlıklı dokulara olabildiğince en az hasarı vermektir. Kemik iliği dozimetrisi kan ölçümlerinden veya nükleer tıp görüntüleme tekniklerinden yararlanılarak iki farklı şekilde yapılabilir. Bu konuda da herhangi standardize edilmiş veya doğruluğu kanıtlanmış bir yöntem bulunmamaktadır. Bu tez çalışmasında kemik iliği dozimetrisi icin görüntü bazlı dozimetri methodu kullanılmıştır. Tez çalışmasına dahil edilen ^{177}Lu[Lu]-PSMA-617 tedavisi uygulanmış metastatik kastrasyona dirençli prostat kanserli hastaların, tedavi sonrası kemik iliği dozları farklı görüntüleme protokolleri kullanılarak hesaplanmıştır. Bu görüntüleme protokolleri çoklu 3D görüntüleri (görüntüleme protokolu 1), çoklu planar görüntüler ile bir adet 3D görüntüsü (görüntüleme protokolu 2), ve tek bir 3D görüntüsü (görüntüleme protokolu 1), kullanılarak oluşturuldu. Üç farklı görüntüleme protokolüne bağlı olarak elde edilen kemik iliği absorbe doz değerleri hem birbirleri ile hem de daha önce yayınlanmış literatür

verileri ile karşılaştırıldı. Bu calışma ^{177}Lu[Lu]-PSMA-617 tedavisi uygulanmış hastalarda 3 farklı görüntü protokolünü kullanıp kişiselleştirilmiş kemik iliği absorbe doz değerlerinin hesaplanıp karşılastırıldığı ilk çalışmadır.

Anahtar Kelimeler: Görüntü bazlı dozimetri, Kemik iliği dozimetrisi, Lutesyum

1. INTRODUCTION

In Nuclear Medicine, the radionuclide treatments can be applied either based on empric approach or dosimetry. Empric approach is a fix-activity based treatment, which relies on the stage of the disease, body weight, body surface area, or general indications stated in the European Medicines Agency (EMA) package insert (1). On the other hand, dosimetry consists of a complete patient-specific treatment planning. Dosimetry explains how a radiopharmaceutical's emissions interact with the patient's body and helps to direct the best clinical use of radiopharmaceuticals (1).

According to European Council Directive 2013/59/Euratom/Article 56, all medical exposures of radiotherapy patients require that exposures of the target volumes must be planned individually and their administration be properly verified, while also ensuring that doses to tissues and non-target volumes are as low as possible and consistent with the exposure's intended radiotherapeutic purpose. (cf. Art. 106 of the basic safety standards).

Dosimetry is listed as optional for standardized therapies and optional or advisable for non-standardized therapies in 2021 based on the European Association of Nuclear Medicine's (EANM) position paper on article 56 of the Council Directive 2013/59/Euratom (2).

The conflict between Euratom/56, EANM position paper might be associated with lack of well-established optimal dosimetry methods. Up to now, there is no multi-center dosimetry studies, which focus to optimise the dosimetry for each specific treatment of nuclear medicine. Nevertheless, many countries in Europe already started to establish the dosimetry protocols especially for the ^{177}Lu-labelled treatments. Associated with the physical properties, ^{177}Lu is one of the radionuclides, which the dosimetry can be performed easily and accurately. ^{177}Lu[Lu]-PSMA-617 is one of the ^{177}Lu labelled treatment, applied in nuclear medicine physicians, has promising treatment responses for the patients with metastatic castration-resistant prostate cancer. In 2022, ^{177}Lu[Lu]-PSMA-617 has FDA approved. Related to ^{177}Lu[Lu]-PSMA-617, the dosimetry was not mentioned in the FDA documents. Nevertheless, 59/Euratom directives, which require dosimetry are clear. In addition, ^{177}Lu[Lu]-PSMA-617 is categorized as non-standardized therapies in the current published EANM position paper (2), which requires the dosimetry too.

In ^{177}Lu[Lu]-PSMA-617 treatment, the red bone marrow is considered as the organ-at-risk. Since the uptake in the red bone marrow is considered to be associated with hepatotoxicity. The highest absorbed dose limit for the red bone marrow was determined as 2 Gy (3, 4).

For ^{177}Lu[Lu]-PSMA-617 treatment, dosimetry can be used to determine the required maximum safe activity of the treatment and also to verify the absorbed doses of the organs at risks as well as tumors.

Red bone marrow dosimetry can be performed based on blood measurements as well as 2D/3D scans (1). Although there are some abstracts mentioned that blood based calculations underestimate the actual red bone marrow absorbed doses compared to the results based on 3D scans, up to now there is no full paper publication showing a direct comparison of blood and imaged based bone marrow dosimetry. Highly associated with the simplicity of the calculations, majority of the publications focusing on the red bone marrow dosimetry were based on blood measurements. In this study, image based approach was used for the red bone marrow dosimetry. Briefly, the image based red bone marrow dosimetry might be summarized by four steps as 2D/3D segmentation, creating the time-uptake curves (TACs), calculating the time integrated activity coefficients (TIACs) and absorbed dose calculations.

There were only three clinical paper related to image based red bone marrow dosimetry, which were published by Svensson et al., Hagmarker et al. and Violet et al. (5,6,7).

In these three articles by Svensson et al., Hagmarker et al. and Violet et al., the image based red bone marrow dosimetry was performed based on multiple 2D planar scans in combination of one 3D scan at 24 h post-injection. Svensson et al. and Hagmarker et al. were performed their studies on [^{177}Lu]Lu-DOTATATE administered patients whereas Violet et al. was performed their study on [^{177}Lu]Lu-PSMA-617 administered patients with metastatic castration resistant prostate cancer.

Svensson et al., Hagmarker et al. and Violet et al. reported the mean absorbed dose per 7.4 GBq values for the red bone marrow as 0.15 – 0.25 Gy/7.4 GBq, 0.32 – 0.46 Gy/7.4 GBq and 0.074-2.52 Gy/7.4GBq, respectively (5,6,7).

All patients in the articles by Svensson et al., Hagmarker et al. and Violet et al. had extent bone metastases. In addition all three studies performed with ^{177}Lu[Lu]-DOTATATE.

In order to full fill the gap of the literature, an image based red bone marrow dosimetry by using 3 different scanning mode was performed for the patients with metastatic castration resistant prostate cancer (who did not have extent bone metastases and who had no tumor in as well as nearby regions of lumbar vertebra 2-4).

2. GENERAL INFORMATION

2.1. Radiation

Radiation is energy transported either by electromagnetic waves (photons) or particles of matter. Basically, radiation is studied in two categories based on its ability to ionize atoms and molecules as ionizing radiation and non ionizing radiation. Non ionizing radiation, has the energy to knock electrons out of atoms' or molecules' orbits.

The non-ionizing radiation does not have the energy to remove an electron from an atom, related to its energy, which is lower than the binding energy of the electron, it cannot form an ion. On the other hand, for ionizing radiation, there is sufficient amount of energy to ionize atoms. Because it ionize atoms and break the structure of atoms, it can cause damage to living cells (8).

Non-ionizing radiation types are radio waves, microwaves, infrared visible light and Ultraviolet. Electromagnetic radiations are described by their frequency, wavelength and energies and the spectrum of electromagnetic radiations are arranged according to these characteristics (9).

Some of the ionizing radiations are alpha particles which are He nucleus (2 protons and 2 neutrons); beta particles (β^-, non-atomic orbital electrons) emitted by an unstable nuclei; protons which is the same as the nucleus of a hydrogen-1 atom have a positive electrical charge; neutrons; positrons ($\beta+$) which are a type of antimatter that eventually interacts with matter in a singular process in which all of their mass is instantly converted to an equivalent quantity of energy in the form of high energy gamma rays; heavy fission fragments (9).

Indirectly ionizing radiation and directly ionizing radiation are the two main categories of ionizing radiation. The target tissue's atoms and molecules' electrons are impacted by direct ionizing radiation. By creating a charged particle (ion or radical) and having that particle interact with orbital electrons, ionizing radiation, which consists of neutral particles, indirectly affects atoms and molecules in a tissue. There are three main types of indirectly ionizing photon radiation: ultraviolet, X-ray, and γ-ray (9).

2.2. Radioactive Decay

Radioactivity is an inherent property of isotopes with unstable nuclei that are expected to remain stable through radioactive decay. The number of protons in the nuclei of all isotopes of a given element is the same, but the number of neutrons varies (10).

The decay process depends on the nucleus in several ways: Alpha decay, beta decay, positron decay, internal conversion, electron capture.

2.2.1. Alpha Decay

Unstable nucleus emits alpha particles, which is a helium nucleus to achieve stability when the nucleus is too large. Alpha particles have +2 charge since they do not have electrons. The number of nucleons reduces by 4 and the atomic number of the nucleus drops by 2, as a result of the emission of an alpha particle from the nucleus. The primary element's physical and chemical characteristics vary when the atomic number changes, transforming it into a different element (10).

$$ {}^{A}_{Z}X = {}^{A-4}_{Z-2}Y + {}^{4}_{2}He \quad (1) $$

2.2.2. Beta Decay

To achieve a stable nucleus, based on the nucleus's protons and neutrons' number, a neutron transforms to a proton or a proton transforms to a neutron.

Proton decay results in the positive charge inside the nucleus decreasing by one, which lessens the attractive forces between protons. However, when a neutron is changed into a proton, the positive charge inside the nucleus rises by one, increasing the repelling forces between protons (10).

β^- Decay occurs when a neutron transforms into a proton in an unstable nucleus. As a result, the number of neutrons reduced and number of protons decreases by one but the total number of nucleons does not change. In this process, an electron and an antineutrino emitted by nucleus and the total energy by this process shared by electron and antineutrino.

$$ {}^{A}_{Z}X = {}^{A}_{Z+1}Y + e^{-} + \bar{\upsilon} \quad (2) $$

2.2.3. Beta Plus Decay

β^+ decay occurs when a proton transforms into a neutron in an unstable nucleus. As a result, the number of protons reduced and number of neutrons decreases by one but the total number of nucleons does not change. In this process, a positron and a neutrino emitted by nucleus and the total energy by this process shared by positron and neutrino (10).

$$ {}^{A}_{Z}X = {}_{Z-1}{}^{A}Y + e^{+} + \upsilon \quad (3) $$

2.2.4. Electron Capture

An electron in an atomic shell is captured by the unstable nucleus during this process, where it combines a proton to create a neutron. A neutrino was released with excess energy, similar to beta decay.

$$ {}^{A}_{Z}X + e^{-} = {}_{Z-1}{}^{A}Y + \upsilon \quad (4) $$

The process of capturing an electron from the K shell of an atom is referred to as K capture; the act of capturing an electron from the L shell is referred to as L capture, and so forth. Electron capture is one of the few instances (another will be encountered in the case of gamma decay) in which a nucleus interacts directly with the orbital (K, L shells, etc.) electrons of an atom. A vacancy is formed in an atom's inner shell when an electron is captured from its K, L, or M shell. Following this vacancy's filling, electrons from higher shells simultaneously emit a characteristic x-ray or Auger electron (10).

2.2.5. Gamma Decay

Gamma decay is a disintegration from excited state to ground state of a nucleus. Generally, it occurs after another radioactive decay for example alpha decay, beta decay, electron capture, because after disintegration nucleus remains in an excited state and emits gamma photon to be stable.

$$ {}^{A}_{Z}X^{*} = {}^{A}_{Z}X + \gamma \qquad (5) $$

2.2.6. Internal Conversion

Instead of producing a γ-ray, a nuclide in an excited state transfers its excess energy straight to an electron in one of the atomic shells (the K, L, or M shell). A nucleus in an excited state emits electrons instead of γ-ray as an alternative, which of these events happens is coincidental. A single nucleus will emit either a γ-ray or an Auger electron. However, in a collection of nuclei, some will emit γ-rays and some conversion electrons (10).

$$ {}^{A}_{Z}X^{*} = {}^{A}_{Z}X + e^{-} \qquad (6) $$

To sum up, a radionuclide decays by losing energy and the time duration taking for a half of the atoms to decay, which is called a radionuclide specific half-life ($T_{1/2}$). The decay proses until the number of atoms reach zero. Eq. 7 represents the decay equation.

$$ \mathrm{A(t)} = \mathrm{A(0)} \cdot e^{-\lambda t} = \cdot e^{-\frac{ln2}{T_{1/2}} \cdot t}\mathrm{A} \qquad (7) $$

Where t is the time point, A(t) is the amount of activity certain time, A(0) is the amount of activity at the initial time point, λ is decay constant and $T_{1/2}$ is the half life

Activity is the number of decays in a unit time. The SI unit of activity is Bq which equals to 1 disintegration per 1 second.

$$ \mathrm{A} = \frac{Number\ of\ Decays}{Time\ (s)} \qquad (8) $$

2.3. Decay Equation

Activity, number of disintegrations in a unit time, based on number of atoms (N) in the radioactive substance and its decay constant.

$$\frac{dN}{dt} = -\lambda N \qquad (9)$$

Therefore, number of decays in a time interval depends on number of atoms at zero time point, decay constant and time elapsed.

$$N(t) = N_0 e^{-\lambda t} \qquad (10)$$

This equation applies directly to the activity.

$$A(t) = A_0 e^{-\lambda t} \qquad (11)$$

The activity of a radionuclide in patients are depends on physical decay and biological elimination. These two processes are independent of each other.

2.4. Physical Half-Life

Physical half-life ($T_{1/2}$) is defined as time requires half of the atoms to disintegrate in a radioactive substance.

2.5. Absorbed Dose

Absorbed dose describes the amount of energy delivered by unit mass (organs, tissues, cells etc.) because of ionizing radiation. The International system of unit for absorbed dose is gray (Gy) which equals to 1 joule per kilogram ($J.kg^{-1}$). Absorbed dose is the desired value to be found by dosimetry because it is a measure of how much tissue damage has been done.

$$\text{Absorbed dose} = \frac{d\varepsilon}{dm} \qquad (12)$$

Energy of an ionizing radiation from a radionuclide equals to number of disintegrations multiply by the energy emitted per one decay (11).

2.6. Radionuclides Used in Nuclear Medicine

In nuclear medicine, single-photon emission computed tomography (SPECT) imaging uses gamma emitter radionuclides and positron emission tomography (PET) imaging uses positron emitter radionuclides for diagnostic purposes. Beta and alpha emitter radionuclides are used for therapeutic purposes in nuclear medicine. In nuclear medicine applications, the radionuclide selection was done primarily based on the chemical and physical characteristics of the preferred radionuclides (10). The most used radionuclides in nuclear medicine might be summarized in Table 2.1.

Table 2.1. Most known radionuclides, which are used in nuclear medicine

Radionuclide	Half-life (h)	Radiation Emission (Probability %)
Positron emitters (PET radionuclides)		
^{18}F	1.83	β^+ (97%)
^{64}Cu	12.7	β^+ (17.8%)
^{68}Ga	1.13	β^+ (89.1%)
^{124}I	100.8	β^+ (22.6%)
Gamma emitters (SPECT radionuclides)		
^{123}I	13.2	γ(87%)
^{99m}Tc	6	γ(91.5%)
^{111}In	67.2	γ(%)
Therapeutic radionuclides		
^{90}Y	64.1	β^- (99.98%)
^{131}I	192.5	β^- (100%)
^{177}Lu	160.8	β^- (100%)
^{225}Ac	238	α (100%)

2.6.1. Properties of Lutetium-177

Lutetium is a chemical element with an atomic number 71. ^{177}Lu has 71 protons and 106 neutrons. It is produced via nuclear reactors.

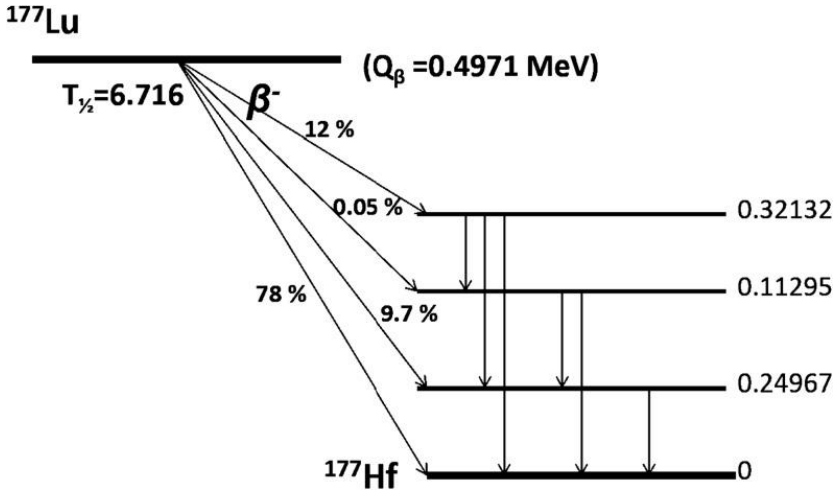

Figure 2.1. Decay scheme of ^{177}Lu

^{177}Lu is a beta emitter to the stable ground state of ^{177}Hf with abundance of 78% with a half-life of 6.7 days. The complete emission list of ^{177}Lu can be seen in table 2.2.

Table 2.2. The radiation emission data of ^{177}Lu

Radiation Type	Mean Energy in keV	Abundance in %
β^-	47.7	11.6
β^-	111.7	9.0
β^-	149.6	79.4
γ	113.0	6.2
γ	208.4	10.4

Nuclear medicine imaging using SPECT is made possible by gamma energies and a distinct gamma peak at 208.3 keV, and the emitted particles are used for therapeutic applications. Soft tissue has an average thickness of 0.7 mm, which prevents healthy tissues from being exposed to high energy radiation. Additionally, ^{177}Lu has a long half life, which allows it to be used for multiple time point imaging, which is necessary to examine the patients' biodistribution, biokinetics, and dosimetry (12).

2.7. Single photon emission computed tomography (SPECT) Imaging

Gamma camera imaging is used in single photon emission computed tomography (SPECT). While a number of 2D images are taken from various angles during SPECT, gamma camera revolves around the patient. How radioactive traces are distributed throughout the body of the patient is then reconstructed in SPECT/CT. When combined with SPECT, computed tomography (CT) shows the connection between anatomies and the functional characteristics of the distribution of the radiopharmaceutical. A CT scan's x-rays are used to create an attenuation map, and with the aid of the map, the attenuation correction for the emitted photons' absorption can be conducted. Then, reconstruction algorithms for SPECT/CT images can integrate the attenuation map (13).

2.7.1. Image Acquisition

Acquisition process is the detection of photons then the conversion to electrical or optical signals. A head or heads of a SPECT system's camera rotate around the patient to capture projection images. The head or heads can move and take scans continuously or they can stop and take images at specified angles that are evenly spaced apart ("step and shoot" acquisition). Pixel size, the selection of the arc, number of angular samples, acquisition duration time at each angle and rotation mode are the parameters, which affect an acquisition of a SPECT scan. It is preffered to collecting high counts for image acquisiton because higher number of counts result in better image quality because of better counting statistics (14,15,16,17). During the acquisition precess, selection of energy window and collimation is very important since they affect sensitivity and spatial resolution. An energy window settings must be selected based on the energy value of photopeak of the used radionuclide to have less effects of scatter. The choice of collimation should also be made appropriately because it affects sensitivity, spatial resolution, signal-to-noise ratio and septal penetration of high-energy photons (18,19).

Incorrect selection of the collimator, for example, not choosing a collimator as thick as it should be, will cause photons penetrating or scattered in the collimator septa to be detected, thus reducing the image contrast and spatial resolution, and increasing image artifacts. (14)

2.7.2. Reconstruction

With the aim of identifying the distribution of the 3D counts that accurately represents the distribution of the activity, which is produced by using a collection of acquired 2D data, tomographic reconstruction is used to obtain the information regarding the distances between the detectors and the photons' starting points. Generating tomographic images from a collection of SPECT projections are done by image reconstruction process. This can be done either iterative or non –iterative reconstruction methods. The non-iterative method image reconstruction method is the filtered back-projection technique and iterative methods called 2D/3D Ordered Subset Expectation Maximization (2D OSEM or 3D OSEM) method. Compared to filtered back-projection technique, iterative methods are superior for quantification. Based on the measured projection data, in an OSEM reconstruction method, the highest likelihood estimate of the tracer distribution is obtained. This technique compares a evaluated projection calculated using knowledge of how a SPECT system operates to a measured projection in the first estimation of a reconstructed image. Bin by bin, an error projection is computed, and the output is backprojected to create an error image. After comparing the data from all projection angles, the first estimate is updated by multiplying it by the error image. Compared to the filtered back-projection approach, 3D OSEM can produce images with higher resolution and contrast (20,21).

The parameters of the applied reconstruction in a SPECT system has an influence on the image noise and the resolution (such as number of iteration/subsets). For instance, for an OSEM based iterative reconstruction, an increase of iterations and subsets increases the spatial resolution, however, it also increases the noise of the image. Therefore, the selection of the number of iterations in reconstruction must be done carefully to represent the reliable activity distribution and count statistics from a sample patient dataset.

Attenuation correction is yet another crucial subject. Attenuation refers to the loss of true event detection as a result of radiation absorption in tissue or as a result of their scattering beyond the detector's field of view. Attenuation depends on depth therefore images that are not attenuation-corrected underestimate activity, particularly in areas deep within the body. Image noise, image artifacts, and image distortion are all increased by the attenuation-related count loss. Data attenuation correction is thus required. In SPECT systems, the attenuation map are generated bya low dose CT and the corrections were performed for the absorption of the emitted photons. The attenuation map can be easily

integrated into iterative reconstruction techniques for SPECT imaging. Similarly a scatter correction could be performed and applied during a reconstruction process. The quantitative effects of scatter are greater at source positions close to the center of the object because the scattered-to-primary-photon ratio grows roughly linearly with source depth. The projection data contain scattered photons, and this causes a spatially variable overestimation of activity in the reconstructed image.

2.7.3. SPECT Camera Sensitivity Factor Calculation

In the calibration process, camera response can be determined by using a phantom with a known amount of activity concentration. It is significant to use the identical settings based on the planned nuclear medicine procedure (same collimator, energy window, and reconstruction settings). The SPECT camera sensitivity factor can be calculated by using the measured total counts of the reconstructed image, during the known acquisition duration time. The unit of a SPECT camera sensitivity factor is represented by counts per second per administered MBq (cps/MBq).

$$\text{Calibration Factor} = \frac{Total\ Counts\ [count]}{Acquisition\ Duration\ time\ [second] x Administered\ Activity\ [MBq]} \quad (13)$$

2.8. Targeted Prostate-Specific Membrane Antigen (PSMA) Radionuclide Radiotherapy for Metastatic Prostate Cancer

Prostate-Specific Membrane Antigen (PSMA) is expressed as a type II transmembrane protein (22). Normal prostate epithelial cells contain PSMA, which is increased in cases of prostate cancer. Expression of the PSMA on prostate cancer cells makes it a useful target for both diagnostic and therapeutic purposes.

In most cases, PSMA labelled with ^{68}Ga is used for diagnostic purposes and ^{177}Lu/ ^{225}Ac labelled PSMA is used for the therapeutic purposes (22).

Currently, [^{68}Ga]Ga-PSMA-11 is the most used radiotracer for PSMA positron emission tomography (PET) imaging in diagnostic applications (22).

[^{68}Ga]Ga-PSMA-11 uses a remarkably simple yet potent molecule, Lys-uriedo-Glu which is attached to a chelating molecule called HBED-CC ((N,N′-bis[2-hydroxy-5-(carboxyethyl)benzyl]ethylenediamine-N,N′-diacetic acid) through a spacer (23).

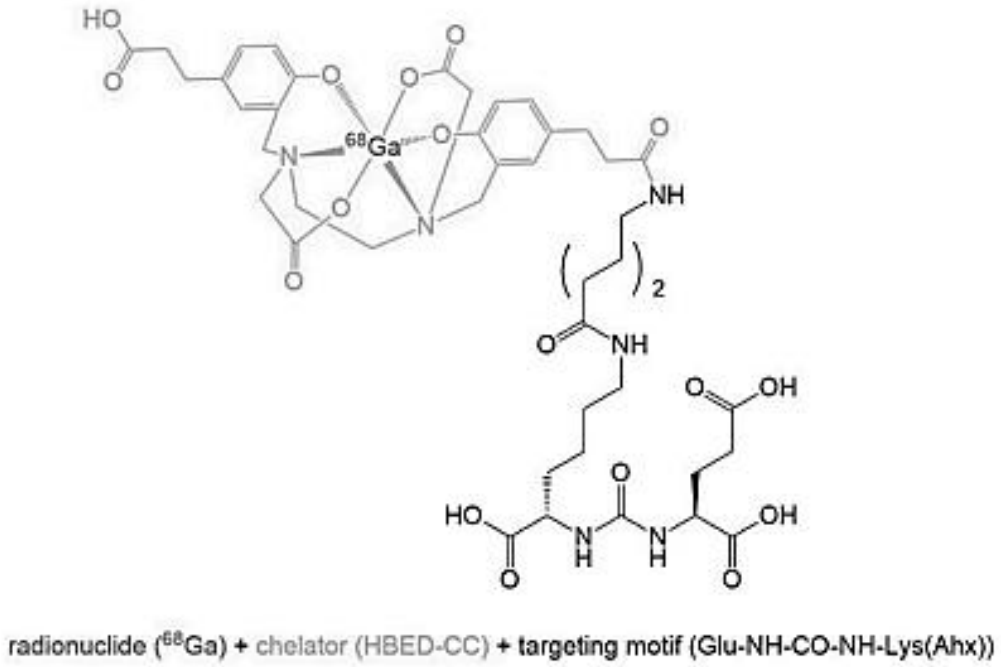

Figure 2.2. Chemical structure of [^{68}Ga]Ga-PSMA-11

PET with PSMA is frequently used in nuclear medicine for theranostic purposes in metastatic castration-resistant prostate cancer (eg., lutetium 177–PSMA radionuclide therapy). PSMA can be labelled with the β^- emitter radionuclides (eg.^{177}Lu) or alpha emitter radionuclides (eg., ^{225}Ac) (17). In soft tissue, due to physical characteristics, ^{177}Lu is the preferred radionuclide for PSMA treatment associated with its physical properties, relatively long half-life, and low energy gamma emission for post-treatment dosimetry analysis (25, 26). Haematological toxicity, or a decrease in bone marrow and blood cells, exposes the patient to infections or may result in anemia, is the radiation toxicity in PSMA therapies labelled with ^{177}Lu that must be taken into consideration.

The same group as [^{68}Ga]Ga-PSMA-11 developed another molecule, PSMA-617(2-[3-(1-Carboxy-5-{3-naphthalen-2-yl-2-[(4-{[2-(4,7,10-tris-carboxymethyl-1,4,7,10-tetraaza cyclododec-1-yl)-acetylamino]-methyl}-cyclohexanecarbonyl)-amino]-propionylamino} pentyl)-ureido]- pentanedioic acid) having DOTA attached to Lys-uriedo-Glu molecule through another linker molecule (23).

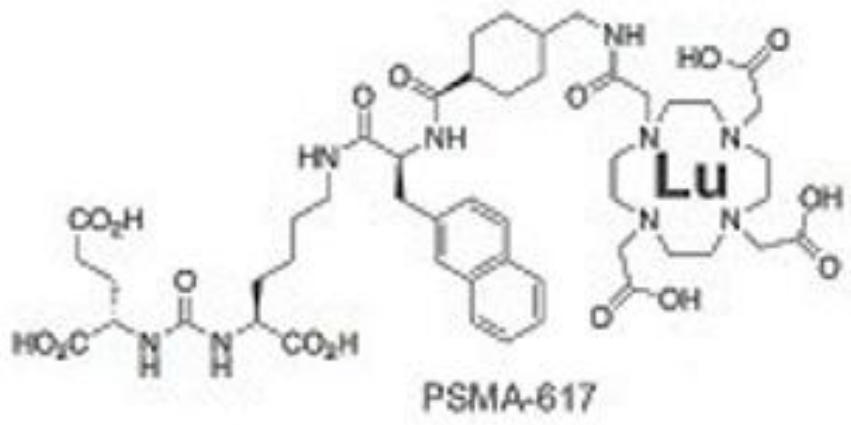

Figure 2.3. Chemical structure of ^{177}Lu[Lu]-PSMA-617 (27)

2.9. Bone Marrow

Bone marrow is located in the cavities of the bones. There are two types of bone marrow: red bone marrow and yellow bone marrow. Red bone marrow is the haematopoietically active part of the bone marrow. It is the part that the blood cells are produced. In an adult, aapproximately one-third of the total bone marrow is red marrow. In adults, 16.1% and 12.3% of total red bone marrow presents in thoracic vertebrae and lumbar vertebrae, respectively. Yellow marrow is not haematopoietically active. It consists mostly fat. (28). Since the main possible toxicity in PSMA labelled ^{177}Lu treatments is haematological toxicity, bone marrow and automatically red bone marrow, where the blood cells are produced is considered as organ-at risk. It is considered that majority of the red bone marrow is located in lumbar vertebrae region (7,20). The maximum tolerable red bone marrow absorbed dose is accepted as 2 Gy. For red bone marrow, dosimetry approaches are not standardized yet. There are still ongoing researches on that topic.

2.10. Dosimetry

The purpose of dosimetry is to provide an effective treatment while ensuring the safety of patients. In other words, it aims to receive maximum amount of harm to the tumors while keeping the dose amount safe to the critical and healthy organs of the treated patient.

Dosimetry can be performed to ensure the safety of applies treatment, to determine the maximum treatment activity (which will be administered to patients) or to optimise the treatment fractions.

Dosimetry can be performed before treatment, during the applied treatment cycles and after the applied treatment.

It is know that dosimetry is not standardized for all of the applications in nuclear medicine and it might be difficult to implement dosimetry in every application in nuclear medicine. However, dosimetry can be performed for the most common treatment of nuclear medicine, which is ^{177}Lu labelled PSMA treatment. In this treatment, the main organ at risk is bone marrow and the^{177}Lu dosimetry can be performed in two different ways based on performed images and based on collected blood samples.

2.10.1. Blood Based Bone Marrow Dosimetry

Blood based dosimetry may depend on only measurement of several blood samples or may depend on 2D WB planar scans in combination of multiple blood samples. Using these measurements, the absorbed doses of the bone marrow can be calculated by using the Medical Internal Radiation Dose (MIRD) formalism (28, 29, 30, 31).

$$D_{bm} = \tilde{A}_{bm} \times S_{bm \leftarrow bm} + \sum \tilde{A}_h \times S_{bm \leftarrow h} + \tilde{A}_{rb} \times S_{bm \leftarrow rb} \quad (14)$$

2.10.2. Image Based Dosimetry

Image based dosimetry can be performed either with multiple 2D scans, multiple 2D scans in combination of one 3D scan, multiple 3D scans, or one single time point 3D scan.

Depending on the selected imaging method, the calculation of absorbed doses can be over- or underestimated. Generally, over- or underestimations of the absorbed doses

associated with 2D scans are caused by organ-count overlays, errors in volume determinations, missing an accurate 2D attenuation correction and errors in 2D background subtractions. 3D scans have advantage due to the absence of overlapping activity contribution, which it results in better image contrast. Additionally, when using SPECT instead of 2D scans, it is more likely due to photon attenuation, scatter contribution, and distance dependent collimator resolution will be accurately corrected (21). The most accurate dosimetry procedure, multiple time point SPECT/CT scans based dosimetry, is regarded as the gold standard for dosimetry. However it is time consuming, therefore the dosimetry is performed based on 2D scans in combination of 3D scan in most of the publications (1).

Image based dosimetry consists of 4 steps as 2D/3D Segment analysis, creation of time-integrated activity curves, calculation of time-integrated activity coefficients and dose calculations.

The absorbed doses might be calculated based on either absorbed dose rates per unit activity (with mass correction) of anthropomorphic phantoms, convolution kernels, or Monte-Carlo simulations (32). Absorbed dose calculations based on convolution kernels and Monte-Carlo simulations require specific software tools. On the other hand, OLINDA/EXM and IDAC-Dose software tools are the most common used software tools, which are available and can be used with no cost to perform organ level dose estimations.

IDAC-Dose 2.1 was developed based on the reference adults in ICRP Publication 133. The software uses the radionuclide decay database from ICRP Publication 107 and takes into account 47 target tissues being exposed to radiation from 83 distinct source regions. In ICRP Publications 60 and 103, the effective dose is described. IDAC-Dose 2.1 can determine the absorbed doses from 1252 different radionuclides of 97 elements (33, 34). In IDAC-Dose software, the absorbed doses and the effective doses were calculated based on input data of time-integrated activity coefficients and administered activity value.

3. MATERIALS and METHODS

In this study, image based bone marrow dosimetry was performed for the patients with metastatic castration resistant prostate cancer by using 3 different scanning modes for the administration of ^{177}Lu[Lu]-PSMA-617.

The TIAC and absorbed dose values calculated by using these 3 image protocols were compared among themselves as well as with the literature.

3.1. Patients

There are two male patients with metastatic prostate cancer in this study. Patient 1 is 68 years old and Patient 2 is 69 years old. Prior to the radionuclide therapy of ^{177}Lu[Lu]-PSMA-617, patient 1 was treated with both chemotherapy and external beam therapy, whereas patient 2 was treated with only chemotherapy. For both patients, a ^{68}Ga[Ga]-PSMA-11 PET/CT scan was performed prior to the ^{177}Lu[Lu]-PSMA-617 administration (see figure 3.1). The administered ^{177}Lu[Lu]-PSMA-617 activities as well as the fraction of the treatment cycles were determined by the nuclear medicine clinician and administered based on the empiric approach cited in the EANM guidelines (administered activity: 8325 MBq for patient 1 treatment cycle 1, 4440 MBq for patient 1 treatment cycle 2 and 5550 MBq for patient 2 treatment cycle 1).

The most important criterion in the selection of patients in this thesis was the absence of tumors in and around the lumbar vertebrae. For all patients, the lumbar vertebra one to five regions (LV1-5) as well as the surrounding regions were tumor free (see figure 3.1).

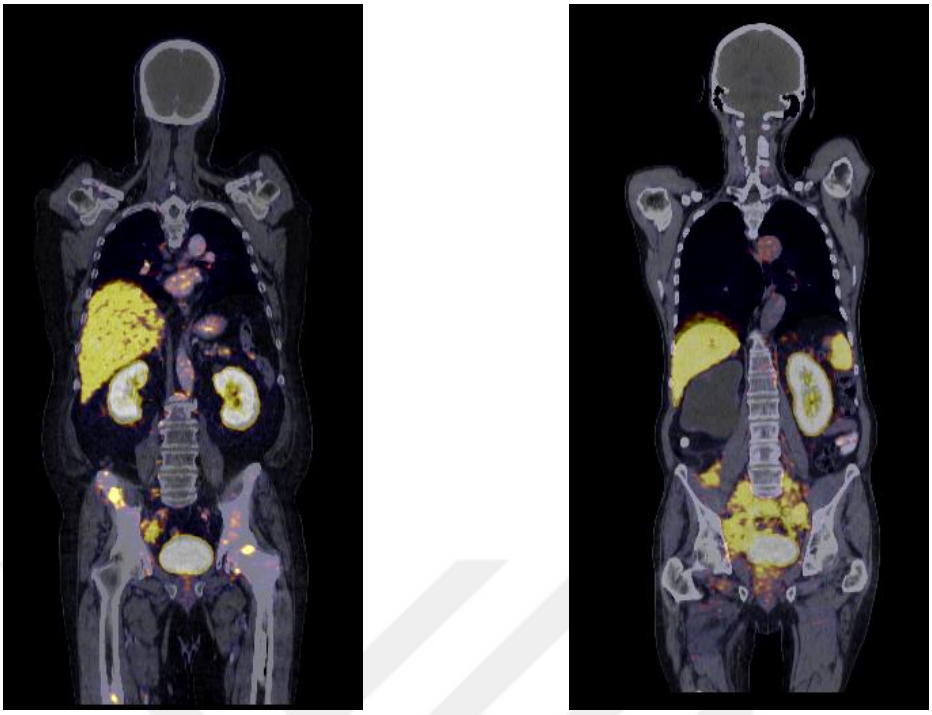

Figure 3.1. The ^{68}Ga[Ga]-PSMA-11 PET/CT Diagnostic Scans of patient 1 (left) and patient 2 (right)

3.2. Image Acquisition and Image Reconstruction

An abdomen 3D scan and sequential WB planar scans were performed in the nuclear medicine department of Yeditepe University Hospital in Turkey at nominally 4, 24, 72/96 (the scans at 96 h post-injection were performed for patient 1 and the scans at 72 h post-injection were performed for patient 2), and 168 hours post-injection of ^{177}Lu[Lu]-PSMA-617. The total scan acquisition duration was 20 min for each abdomen 3D scan and 7 min for each WB planar scan post-injection.

Figure 3.2. Image of Ge Discovery NM/CT 670 Pro SPECT/CT camera used in this study

Medium energy general purpose collimator (MEGP) was used for the collimation. The energy window range was in the range of 187.2–228.8 keV.

For the 3D scans post-injection, the reconstruction was performed by applying 3D OSEM with 2 iterations and 10 subsets. The Butterworth filter with a cut-off frequency of 0.5 and an order of 10 was applied for the 3D scans. A low dose CT (120 kVp with 20 mAs) was acquired for the attenuation correction, and dual energy window based scatter correction (144-176 keV) was applied for the 3D scans.

The details of the applied 2D attenuation and background corrections were explained in the section 'Dosimetry Analysis'.

The camera sensitivity factor was 501.05 counts per second per MBq for the GE Discovery NM/CT 670 Pro 3D camera.

3.2.1. Scanning modes used for Dosimetry

Three different scanning modes were tested for the red bone marrow dosimetry of ^{177}Lu[Lu]-PSMA-617.

The first scanning mode was based on multiple 3D scans, which included four sequential 3D scans at nominally 4, 24, 72/96, and 168 h (see figure 3.3).

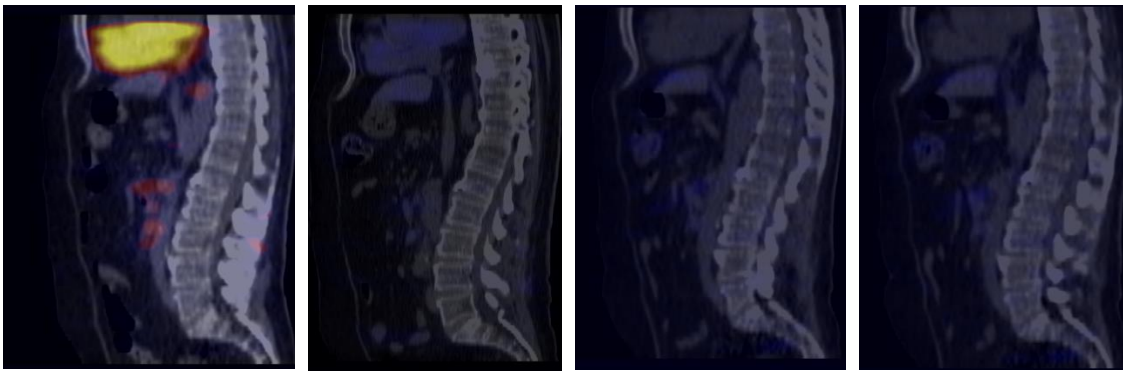

Figure 3.3. 3D scans of patient 1 for the treatment cycle 1 at nominally 4, 24, 96 and 168 h post-injection

The second scanning mode was based on multiple planar scans at nominally 4, 24, 72/96, and 168 h post-injection in a combination of one abdomen 3D scan post-injection (see figure 3.4). The second scanning mode was tested by using each performed 3D scan at 4, 24, and 168 h post-injection for patient 1, and at 4, 72 and 168 h post-injection for patient 2, since the CT scans at 96 h and 24 h were not available for patient 1 and patient 2, respectively.

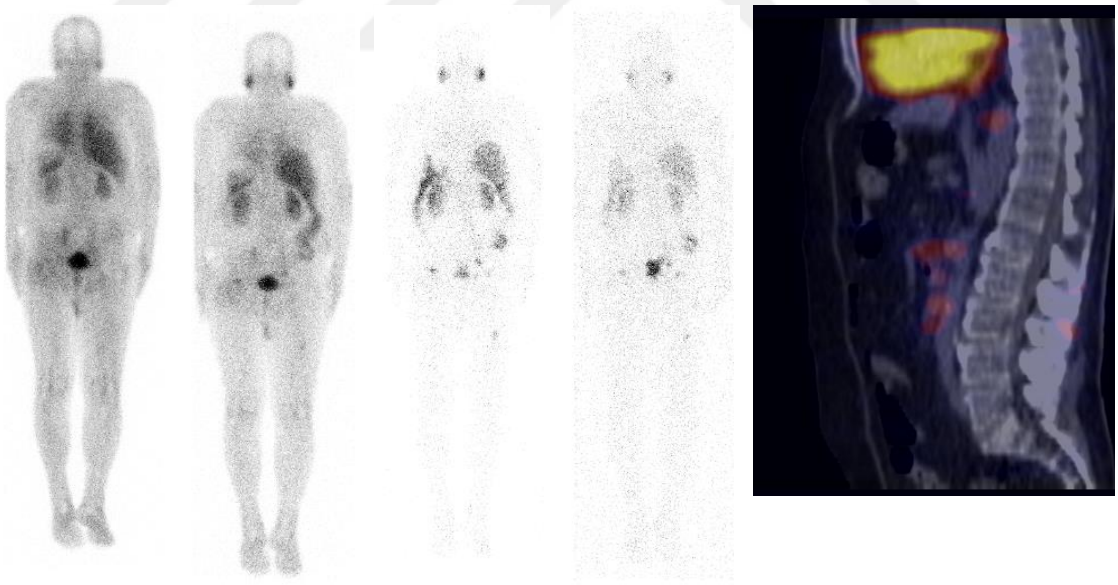

Figure 3.4. The performed WB planar scans of patient 1 for the first treatment cycle at 4, 24, 96 and 168 h post injection including the sagittal axis abdomen 3D scan at 24 h post-injection

The third scanning mode was based on a single 3D scan post-injection. The third scanning mode was tested by using each performed 3D scan at 4, 24, 72, 96, and 168 h post-injection.

3.2.2. Dosimetry Analysis

The total number of counts was calculated based on the drawn 2D and 3D segments of the performed WB planar scans and the 3D scans, respectively (see figures 3.5 and 3.6). All segmentation procedures were performed via a special segmentation software program, which was developed for research purposes.

For the scanning mode 1, in the software, the transfer of the drawn volume of interests are possible. For instance, although the CT scans at 24 h and 96 h post-injection are missing, the drawn segments combined with the CT scans performed at different time points could be used in combination with the SPECT scans at 24 h and 96 h post-injection for segmentation. However, the same procedure could not be performed for the scanning mode 2. Since in this module of the software, the loaded SPECT and CT scans are required to have the same acquisition day. Therefore, the analysis related to the scanning mode 2, including the 3D scans at 24 h and 96 h post-injection, couldn't be performed.

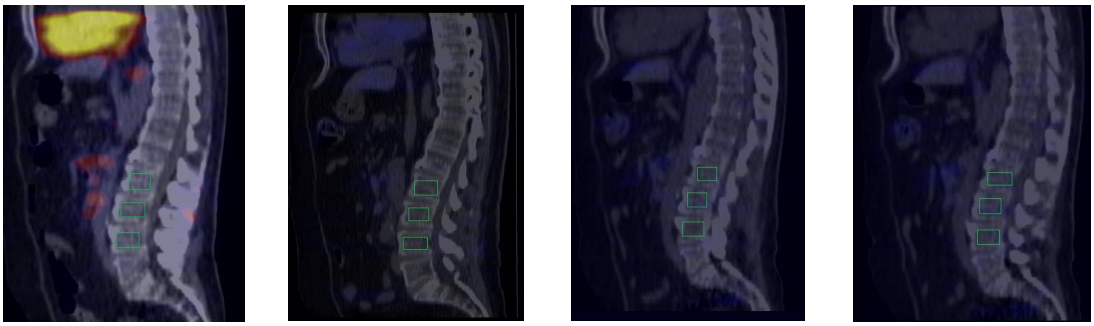

Figure 3.5. The drawn 3D segments of lumbar vertebra 2-4 on the 3D scan at 4, 24, 96 and 168 h post-injection for patient 1

For the scanning mode 1, the 3D segments of the LV2-4 were delineated based on the CT scans. The activity concentrations were calculated by applying the 3D camera sensitivity factor (501.05 cpm/MBq).

For the scanning mode 2, the four 2D segments for the WB, the WB background (WBBG), the LV2-4, and the LV2-4 background were drawn on the WB planar scans

(see figure 3.6). Then the geometric mean based attenuation correction and the background subtraction correction were applied (1). The count rates of the 2D segments were normalized to the absolute activity concentrations based on the 3D segment.

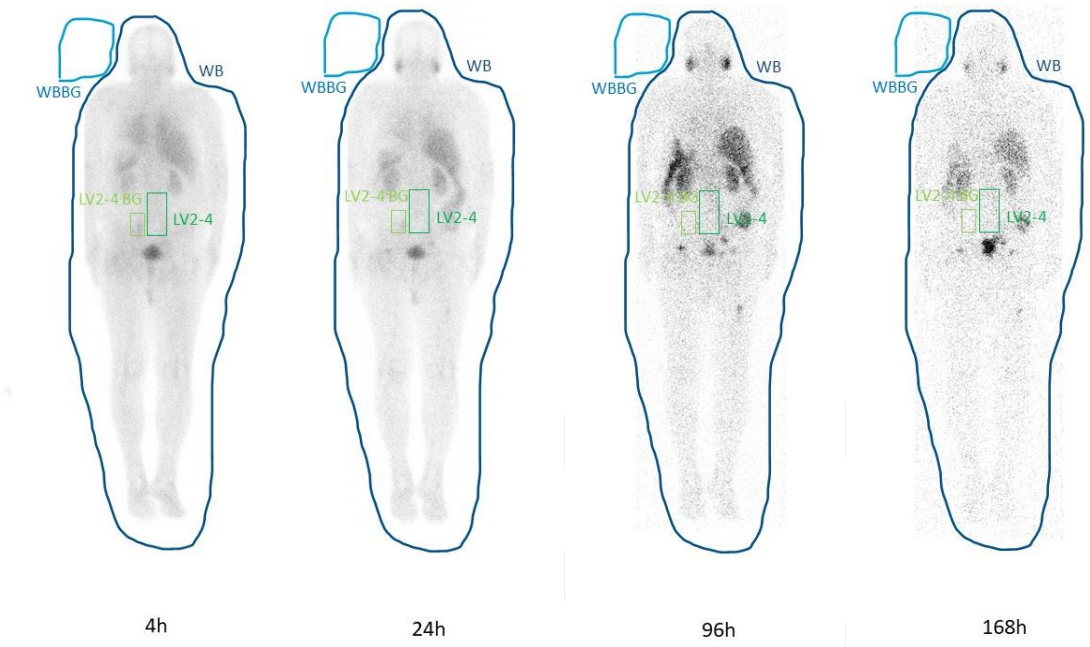

Figure 3.6. The drawn 2D segments of the WB (dark blue coloured), the WB background (light blue coloured), the lumbar vertebrae 2-4 (dark green coloured) and the lumbar vertebrae 2-4 background (light green coloured) on the WB planar scans at 4, 24, 96 and 168 h post-injection for patient 1

Based on the information coming from 2D and 3D segments, the uptakes versus scan time points post-injection were calculated and the corresponding percentage uptake versus scan time point curves were created (see figure 3.9).

3.2.3. Time-Integrated Activity Coefficient (TIAC) Calculation

Time-integrated activity coefficient (TIAC) values of the drawn LV2-4 regions were calculated by NUKFIT software (35). The calculated percentage uptake for each scan time point post-injection was used as input data for NUKFIT. Then the 10% Gaussian error propagation and the optimal fit function suggested by NUKFIT were selected to integrate the TACs. As a result of the integration, TIACs were calculated.

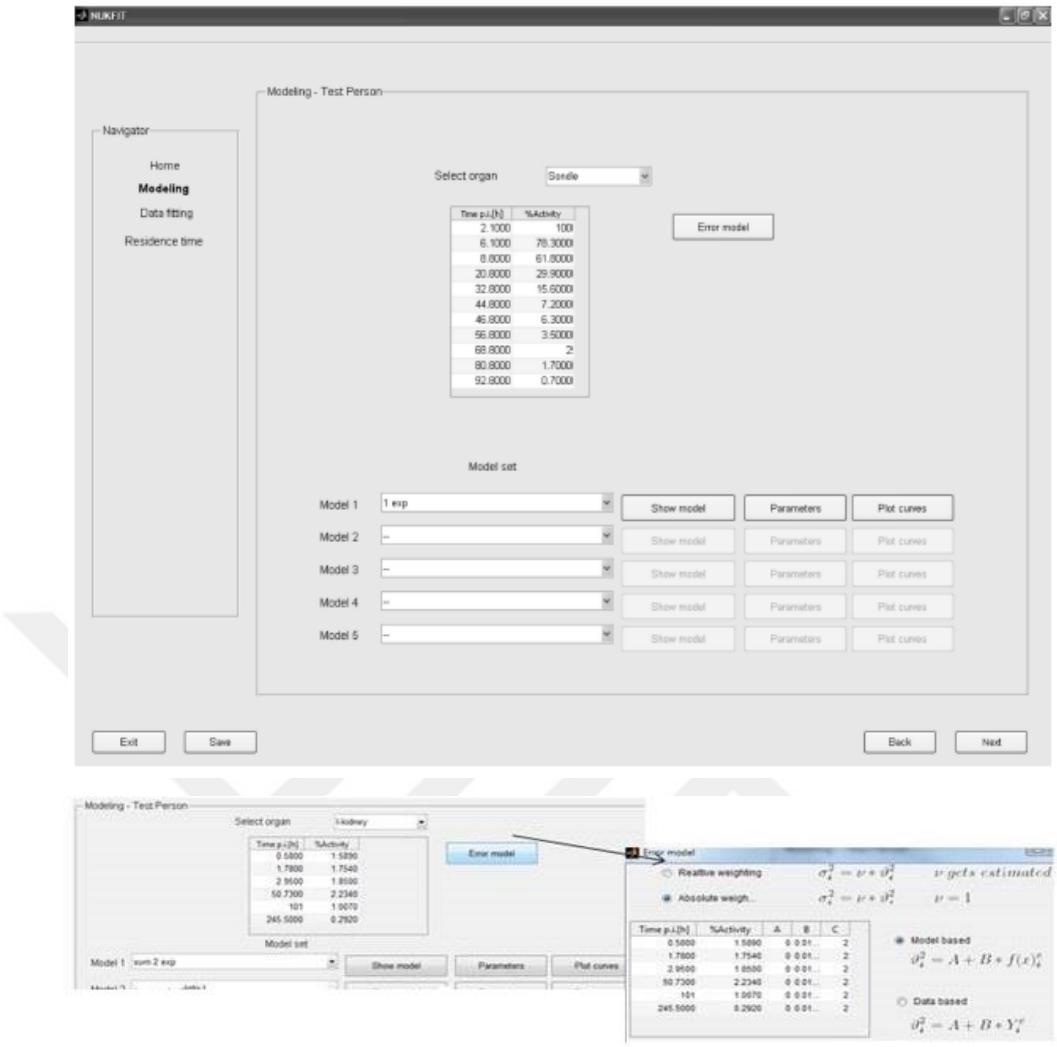

Figure 3.7. NUKFIT error model selection

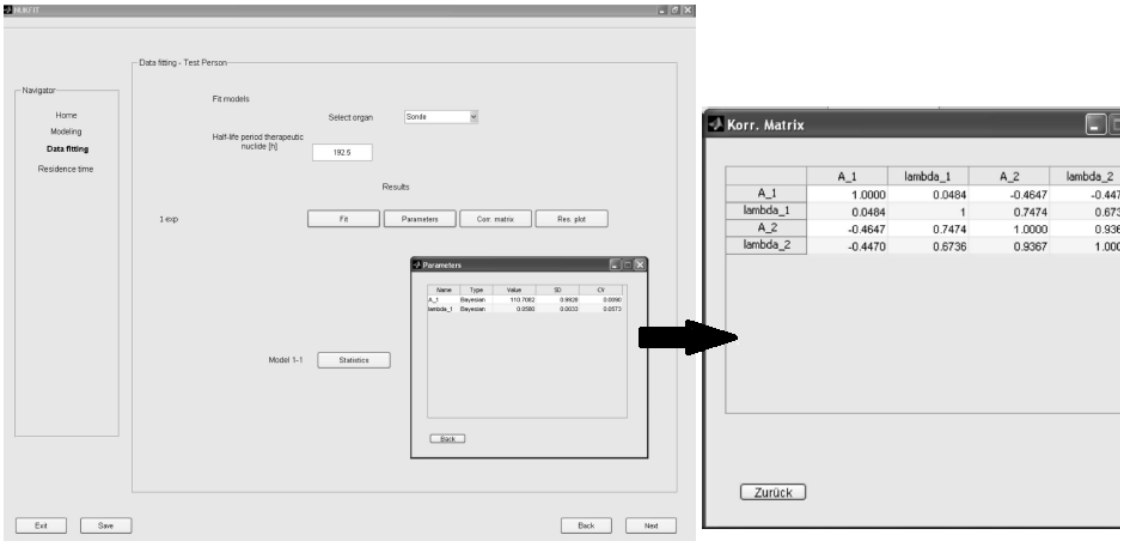

Figure 3.8. NUKFIT fitting parameters

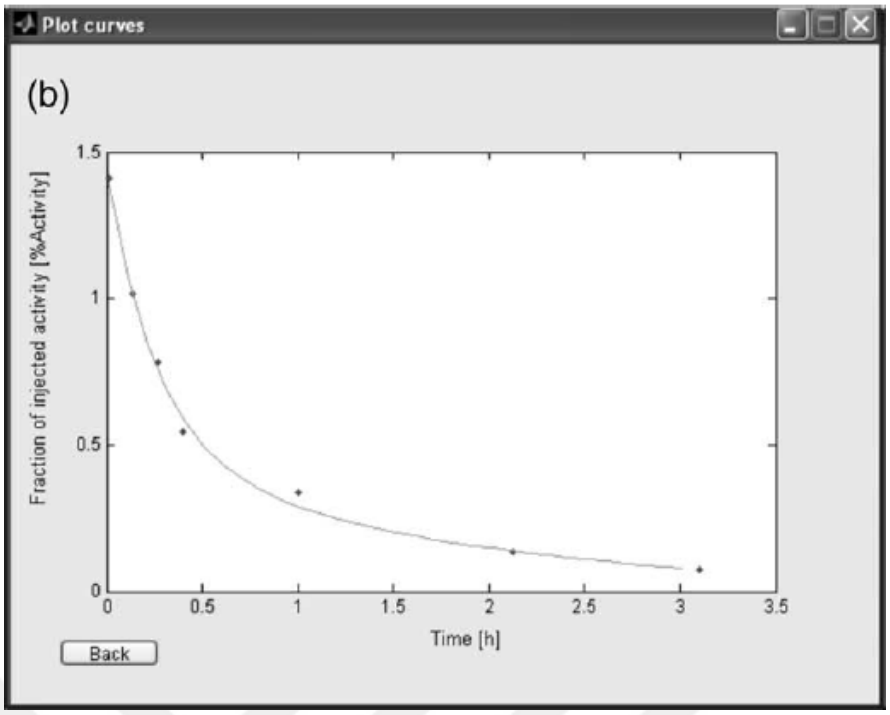

Figure 3.9. NUKFIT plot curves (fraction of injected activity represents the percentage uptake)

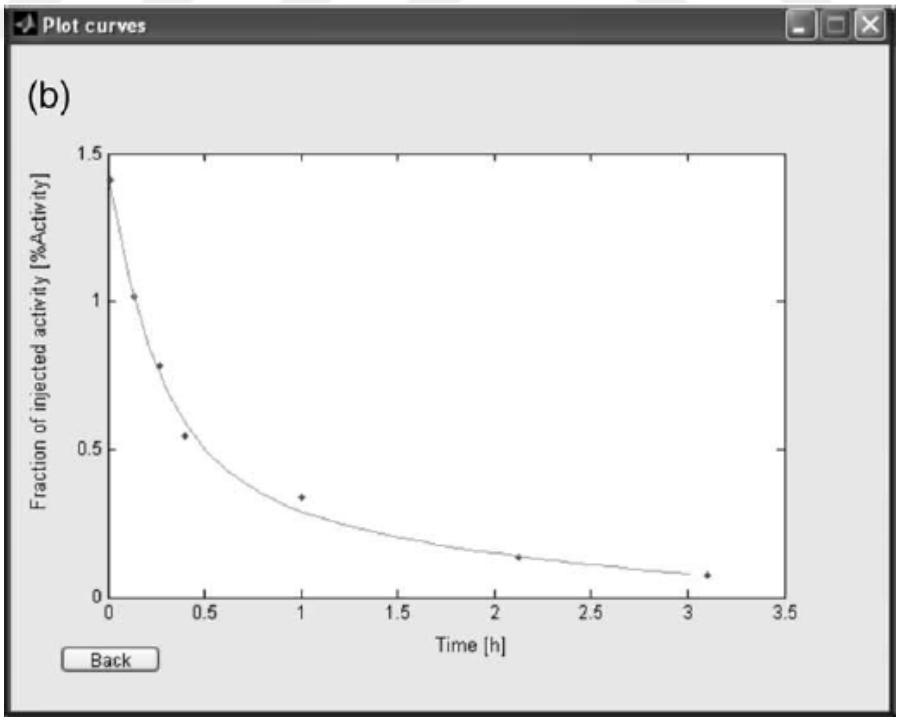

Figure 3.10. NUKFIT plot curves (fraction of injected activity represent percentage uptake)

The optimal fit function suggested by NUKFIT for all patients in each treatment cycle was mono-exponential plus the physical decay (see Equation 14).

$$\mathrm{A}_1 e^{-(\lambda_1 + \lambda_{phys})t} + A_2 e^{-(\lambda_{phys})t} \quad (15)$$

The TIACs of the total red bone marrow were estimated by using the TIACs of LV 2-4 with the knowledge: 6.7% of the total red bone marrow is represented by LV2-4 in a human body (28) (see Equation 15).

$$\mathrm{TIAC}_{\text{red bone marrow}} \cong \frac{\mathrm{TIAC}_{\mathrm{LV2-4}}}{0.067} \quad (16)$$

3.3. Absorbed Dose

3.3.1. Absorbed dose calculations for scanning modes 1 and 2

For scanning modes 1 and 2, the absorbed doses of the LV 2-4 and the bone marrow were calculated by using IDAC-Dose 2.1 software (33). The estimated TIACs were used as input values for IDAC-Dose 2.1. After selecting the radionuclide and entering the TIACs as input values, the used radionuclide and the amount of administered treatment activity values were adjusted to calculate the patient specific absorbed doses. The ICRP 110 adult computational voxel male phantom was selected for the calculations, and the patient specific CT based LV 2-4 volumes were used. The patient specific CT based LV 2-4 volumes were measured by drawing 3D segments on CT images of the patients. Scaled TIACs (see Equation 15) were used for the red bone marrow absorbed dose calculations, which were based on scanning modes 1 and 2.

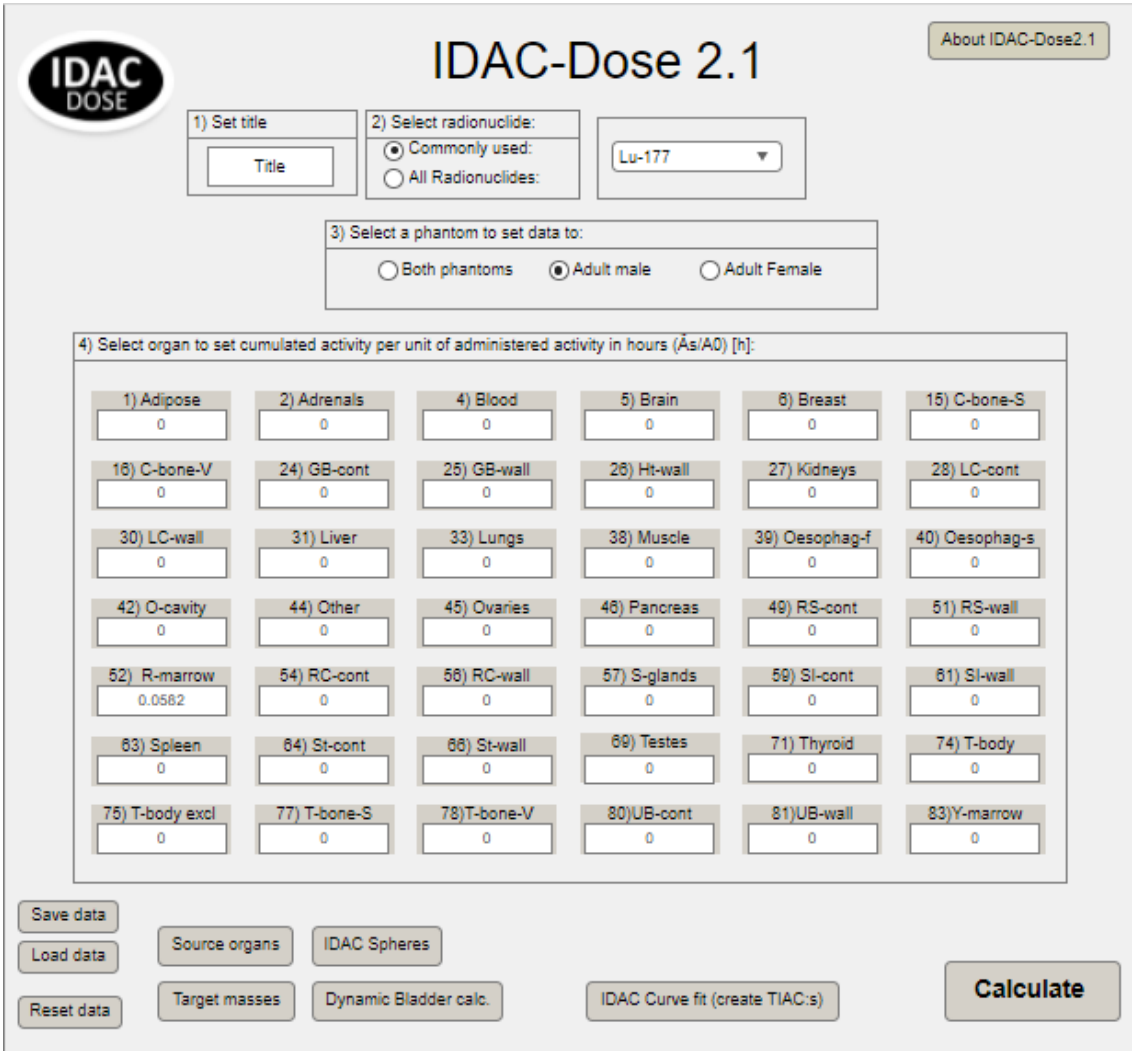

Figure 3.11. IDAC-Dose 2.1. Software screenshot

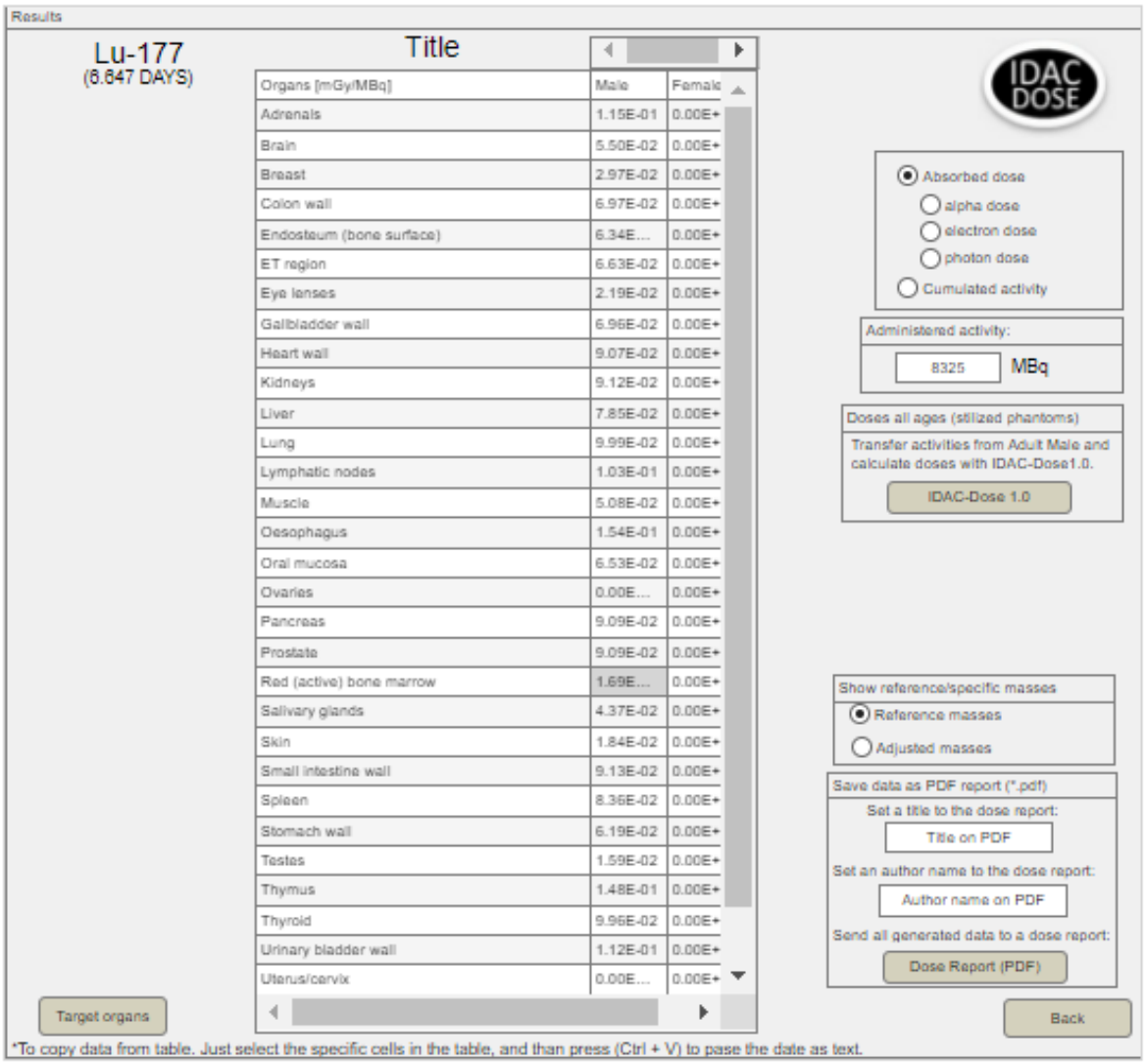

Figure 3.12. IDAC-Dose 2.1. based absorbed doses for patient 2

3.3.2. Absorbed dose calculations for scanning mode 3

For the scanning mode 3, equation 16 was only used to calculate the absorbed doses of the LV 2-4. The scanning mode 3 based absorbed dose calculations were not performed for the red bone marrow.

A constant factor of 0.25 Gy·g/MBq/h constant in the formula allows us to calculate the absorbed dose using the bone marrow mass and analysis data with 3D scans.

It was defined by Hänscheid H. et al. for spherical objects with masses between 10 g and 1 kg with an uncertainty of 2% (1).

Equation 3 is suggested to be used in the case where the value of 3D scan time after the injection per effective half-life is (t_{scan}/T_{eff}) is in the range of 0.75 and 2.5 (36).

$$\text{Absorbed Dose} \cong \left(0.25\ \frac{\text{Gy.g}}{\text{MBq}\cdot\text{h}}\right) \times \frac{\text{total counts} \times \text{scan time}}{\text{acquisition duration} \times \text{organ mass} \times \text{camera sensitivity factor}} \quad (17)$$

Where:

- Total Counts (unit: counts): Total number of counts in the drawn 3D segment
- Scan time (unit: h): Time elapsed post-injection
- Acquisition duration (unit: h): Total acquisition duration of the SPECT scan post-injection
- Organ mass (unit: cm^3): Patient-specific CT based volume
- Camera Sensitivity Factor: Sensitivity factor of the 3D camera (unit: counts per second per MBq)

4. RESULTS

The analysis of the biodistribution and the calculated TIACs of the LV2-4 was performed. Time-uptake curves of the LV2-4 were created by using scanning mode 1 and scanning mode 2, and corresponding TIACs were reported. The calculated TIACs based on scanning modes 1 and 2 were compared and the mean relative differences were reported with the scanning mode 1 based results as reference. The calculated TIACs based on scanning modes 1 and 2 were used for the absorbed dose calculations of the LV2-4. The relative differences in the absorbed doses of the LV2-4 between the three scanning modes were reported (taking scanning mode 1 based results as reference).

In addition, the examinations of the absorbed doses of the red bone marrow was also calculated by using two different scanning modes. The TIACs of the LV2-4, calculated based on scanning mode 1 and 2, were used to estimate the absorbed doses of the red bone marrow (by applying a scale factor, Equation 2). The relative difference in the red bone marrow absorbed doses between the two scanning modes was reported (taking scanning mode 1 based results as reference).

4.1. Biodistribution

The calculated percentage uptakes of the LV2-4 region versus scan time points post-injection can be seen in figure 4.1.

Based on the comparison to the time-percentage uptake curves based on the scanning mode 1, the most similar percentage uptake distribution was obtained by using scanning mode 2 including the 3D scan at 4 and 24 h post-injection, whereas the highest discrepancy was observed by using scanning mode 2 including the 3D scan at 168 h post-injection.

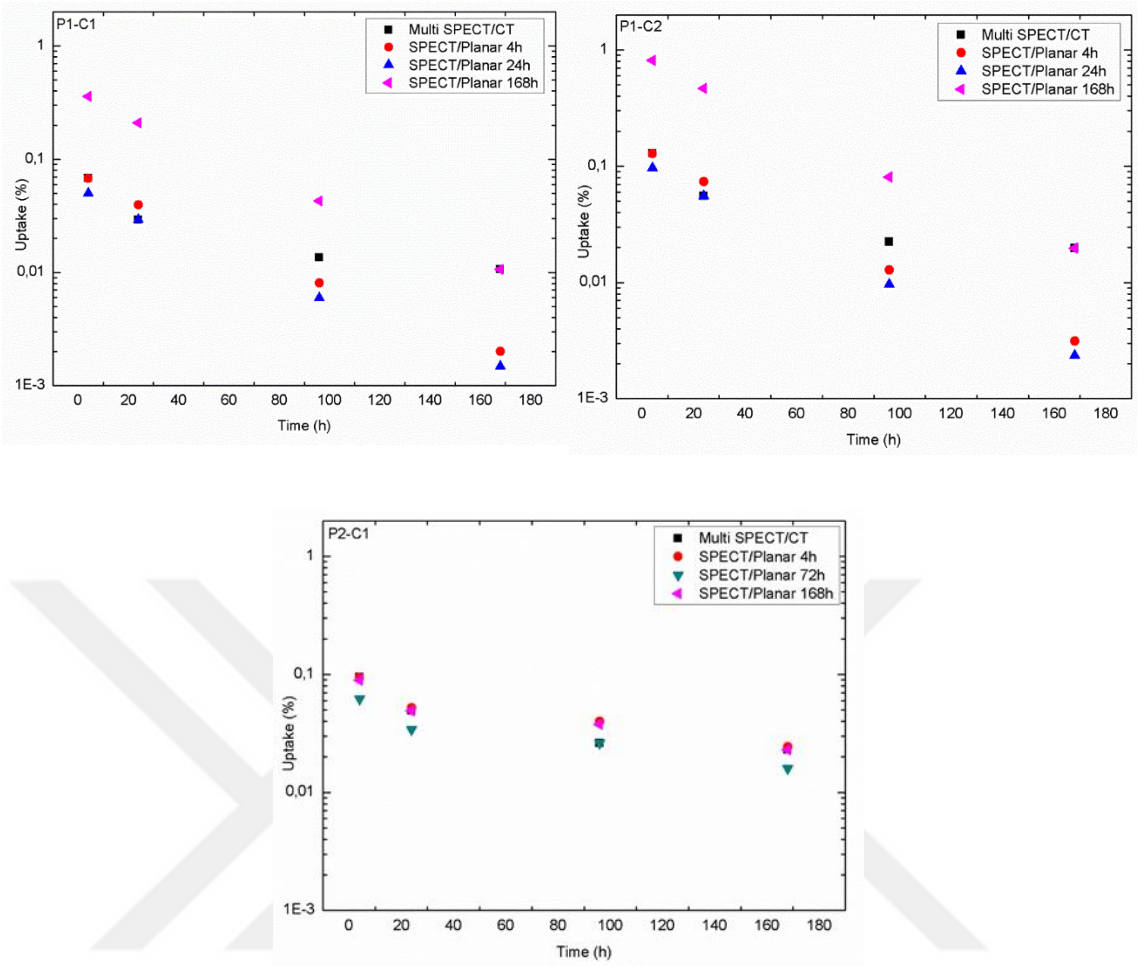

Figure 4.1. Percentage uptake versus scan time points post-injection for each patient in each treatment cycle concerning the lumbar vertebrae 2-4

(P1-C1: patient 1- treatment cycle 1, P1-C2: patient 1- treatment cycle 2, P2-C1: patient 2- treatment cycle 1. Multi 3D: scanning mode 1 including multiple 3D scans, SPECT/Planar 4 h: the scanning mode 2 including multiple planar scans in combination of one abdomen 3D scan at 4 h post-injection, SPECT/Planar 24 h: the scanning mode 2 including multiple planar scans in combination of one abdomen 3D scan at 24 h post-injection, SPECT/Planar 72 h: the scanning mode 2 including multiple planar scans in combination of one abdomen 3D scan at 72 h post-injection, SPECT/Planar 168 h: the scanning mode 2 including multiple planar scans in combination of one abdomen 3D scan at 168 h post-injection)

4.2. Time-Integrated Activity Coefficients (TIACs)

LV2-4 TIAC analysis:

The calculated mean TIAC of the LV2-4 was 0.08±0.02 for the scanning mode 1, 0.07±0.05 for the scanning mode 2 including the 3D scan at 4 h post-injection, 0.06±0.03 for the scanning mode 2 including the 3D scan at 24/72 h post-injection, and 0.25±0.12 for 168 h of scanning mode 2 (see figure 4.2). For the treatment cycles 1 and 2 of patient 1, the lowest relative difference in the TIACs between scanning modes 1 and 2 was calculated by using scanning mode 2, including the 3D scan at 4/24 h post-injection as <-54%.

Compared to the scanning mode 1 based TIACs of the LV2-4, the scanning mode 2 based TIACs including a 3D scan at 4, 72, and 168 h post-injection resulted in <±24% relative difference. The relative difference in the calculated TIACs of the LV2-4 for the patients in each treatment cycle, taking reference scanning mode 1, can be seen in table 4.1.

Table 4.1. The relative difference in the calculated TIACs of the LV2-4 for the patients in each treatment cycle, taking reference the scanning mode 1

Method	**Relative difference compared to scanning mode 1 (%)**
Scanning mode 2 including 3D scan at 4 h	-43 – +27
Scanning mode 2 including 3D scan at 24/72 h	-59 – -16
Scanning mode 2 including 3D scan at 168 h	+21 – +269

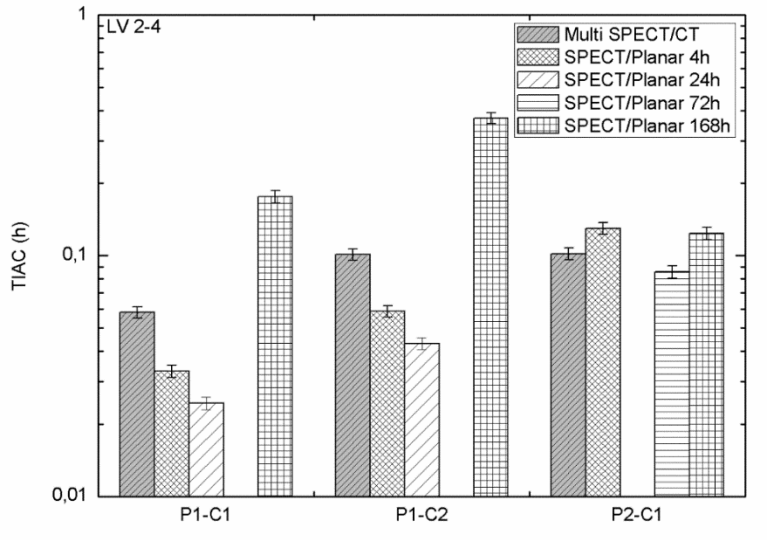

Figure 4.2. The time-integrated activity coefficients (TIACs) of lumbar vertebrae 2-4 for the patients in each treatment cycle based on different scanning modes (P1-C1: patient 1- treatment cycle 1, P1-C2: patient 1- treatment cycle 2, P2-C1: patient 2- treatment cycle 1. Multi 3D: scanning mode 1 including multiple 3D scans, SPECT/Planar 4 h: the scanning mode 2 including multiple planar scans in combination of one abdomen 3D scan at 4 h post-injection, SPECT/Planar 24 h: the scanning mode 2 including multiple planar scans in combination of one abdomen 3D scan at 24 h post-injection, SPECT/Planar 72 h: the scanning mode 2 including multiple planar scans in combination of one abdomen 3D scan at 72 h post-injection, SPECT/Planar 168 h: the scanning mode 2 including multiple planar scans in combination of one abdomen 3D scan at 168 h post-injection)

For the red bone marrow, the calculated mean TIAC was 1.19±0.33 h for the scanning mode 1, 22±0.72 h for the scanning mode 2 including the 3D scan at 4 h post-injection, 0.82±0.46 for the scanning mode 2 including the 3D scan at 24/72 h post-injection, and 3.71±1.86 for the scanning mode 2 including the 3D scan at 168 h post-injection (see figure 4.3).

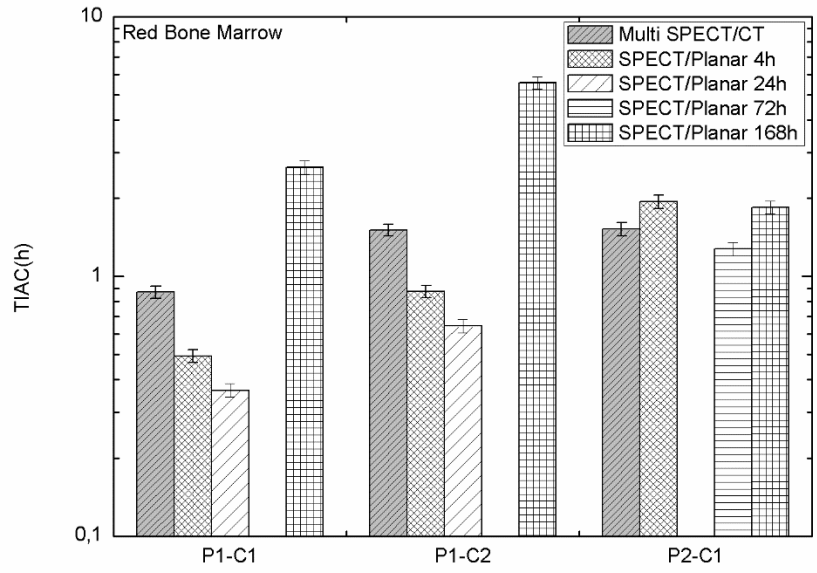

Figure 4.3. The time-integrated activity coefficients (TIACs) of the red bone marrow for the patients in each treatment cycle based on different scanning modes (P1-C1: patient 1- treatment cycle 1, P1-C2: patient 1- treatment cycle 2, P2-C1: patient 2- treatment cycle 1. Multi 3D: scanning mode 1 including multiple 3D scans, SPECT/Planar 4 h: the scanning mode 2 including multiple planar scans in combination of one abdomen 3D scan at 4 h post-injection, SPECT/Planar 24 h: the scanning mode 2 including multiple planar scans in combination of one abdomen 3D scan at 24 h post-injection, SPECT/Planar 72 h: the scanning mode 2 including multiple planar scans in combination of one abdomen 3D scan at 72 h post-injection, SPECT/Planar 168 h: the scanning mode 2 including multiple planar scans in combination of one abdomen 3D scan at 168 h post-injection)

4.3. Absorbed Dose per Unit Activity (Gy/GBq)

The calculated mean absorbed dose per administered activity value of the LV2-4 was 0.05±0.02 Gy/GBq for the scanning mode 1.

The calculated mean absorbed dose per administered activity value of the LV2-4 was 0.05±0.04 Gy/GBq for the scanning mode 2 including the scanning mode 1 including the 3D scan at 4 h post-injection, 0.03±0.01 Gy/GBq for the scanning mode 2 including the 3D scan at 24 h post-injection, 0.06 Gy/GBq for the scanning mode 2 including the

3D scan at 72 h post-injection and 0.16±0.08 Gy/GBq for the scanning mode 2 including the 3D scan at 168 h post-injection (see figure 4.4).

For scanning mode 3, the calculated mean absorbed dose per activity value of the LV2-4 was 0.02±0.01 Gy/GBq where the scanning mode 1 including the 3D scan at 4 h post-injection was used; 0.03±0.01 Gy/GBq where the scanning mode 2 including the 3D scan at 24 h post-injection was used; 0.05±0.02 Gy/GBq where the scanning mode 2 including the 3D scan at 72/96 h post-injection was used; and 0.10±0.04 Gy/GBq where the scanning mode 2 including the 3D scan at 168 h post-injection is used (see figure 4.4).

Taking reference to the absorbed doses of the LV2-4, which were calculated based on scanning mode 1, the scanning mode 3 including the 3D scan at 72 h and 96 h post-injection resulted in the most similar results (the range of relative difference in percent: -4% – +18%). Compared to the scanning mode 1 based absorbed doses of the LV2-4, the highest mean relative differences were calculated for the scanning mode 2 including the 3D scan at 168 h post-injection and the scanning mode 3 including the 3D scan at 168 h post-injection as 269% and 98%, respectively.

The calculated mean absorbed dose per administered activity value of the red bone marrow was 0.04±0.01 Gy/GBq for the scanning mode 1, 0.05±0.03 Gy/GBq for the scanning mode 2 including the 3D scan at 4 h post-injection, 0.02±0.01 Gy/GBq for the scanning mode 2 including the 3D scan at 24 h post-injection, 0.04 Gy/GBq for the scanning mode 2 including the 3D scan at 72 h post-injection, and 0.13±0.06 Gy/GBq for the scanning mode 2 including the 3D scan at 168 h post-injection.

Taking reference to the absorbed doses of the red bone marrow, which were calculated based on the scanning mode 1, the scanning mode 2 including the 3D scan at 4 h post-injection resulted in the most similar results for patient 1 (relative difference: < -43%) whereas the scanning mode 2 including the 3D scan at 72 h post-injection resulted in the most similar results for patient 2 (relative difference: < -17%). The highest relative differences were calculated for the scanning mode 2, including the 3D scan at 168 h post-injection (the range of relative difference: 236±34%)

The relative differences in the calculated absorbed doses of the LV2-4 and the red bone marrow for the patients in each treatment cycle, taking reference scanning mode 1, can be seen in figure 4.6 and figure 4.7, respectively.

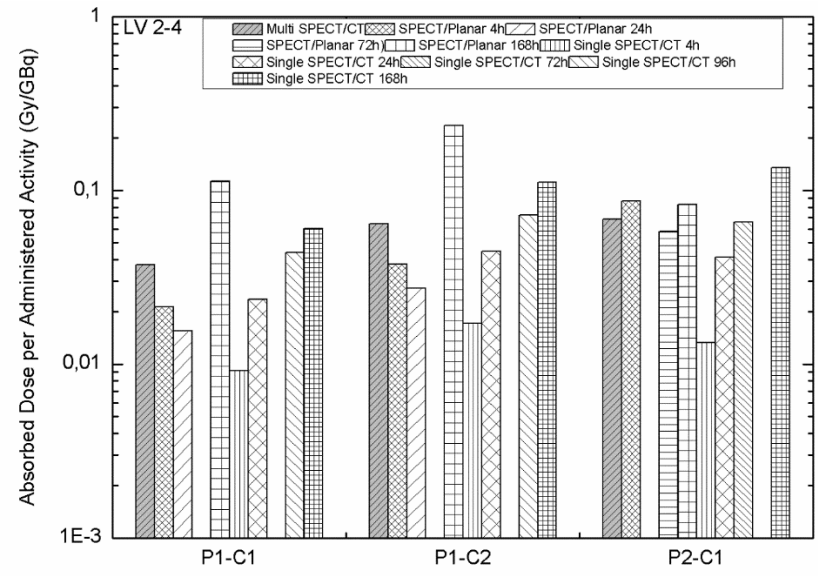

Figure 4.4. The absorbed dose per administered activity values of lumbar vertebra 2-4 for the patients in each treatment cycle

(P1-C1: patient 1- treatment cycle 1, P1-C2: patient 1- treatment cycle 2, P2-C1: patient 2- treatment cycle 1, Multi 3D: scanning mode 1 including multiple 3D scans; SPECT/Planar 4 h: the scanning mode 2 including multiple planar scans in combination of one abdomen 3D scan at 4 h post-injection, SPECT/Planar 24 h: the scanning mode 2 including multiple planar scans in combination of one abdomen 3D scan at 24 h post-injection, SPECT/Planar 72 h: the scanning mode 2 including multiple planar scans in combination of one abdomen 3D scan at 72 h post-injection, SPECT/Planar 168 h: the scanning mode 2 including multiple planar scans in combination of one abdomen 3D scan at 168 h post-injection; Single 3D 4 h: scanning mode 3 including one 3D scan at 4 h, Single 3D 24 h: scanning mode 3 including one 3D scan at 24 h, Single 3D 72 h: scanning mode 3 including one 3D scan at 72 h, Single 3D 96 h: scanning mode 3 including one 3D scan at 96 h, Single 3D 168 h: scanning mode 3 including one 3D scan at 168 h.)

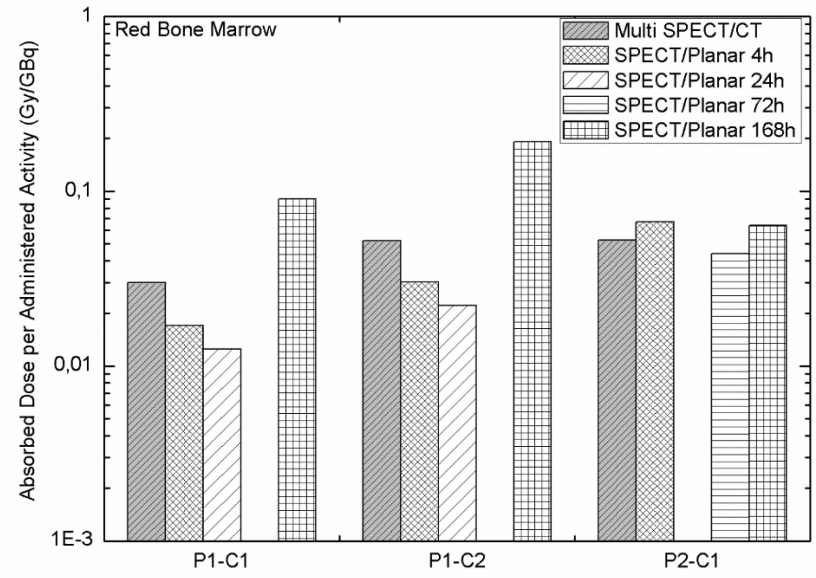

Figure 4.5. The absorbed dose per administered activity values of the red bone marrow for the patients in each treatment cycle

(P1-C1: patient 1- treatment cycle P1-C1: patient 1- treatment cycle 1, P1-C2: patient 1- treatment cycle 2, P2-C1: patient 2- treatment cycle 1, Multi 3D: the scanning mode 1 including multiple 3D scans, SPECT/Planar 4 h: the scanning mode 2 including multiple planar scans in combination of one abdomen 3D scan at 4 h post-injection, SPECT/Planar 24 h: the scanning mode 2 including multiple planar scans in combination of one abdomen 3D scan at 24 h post-injection, SPECT/Planar 72 h: the scanning mode 2 including multiple planar scans in combination of one abdomen 3D scan at 72 h post-injection, SPECT/Planar 168 h: the scanning mode 2 including multiple planar scans in combination of one abdomen 3D scan at 168 h post-injection)

4.4. Relative difference in Gy/GBq compared to scanning mode 1

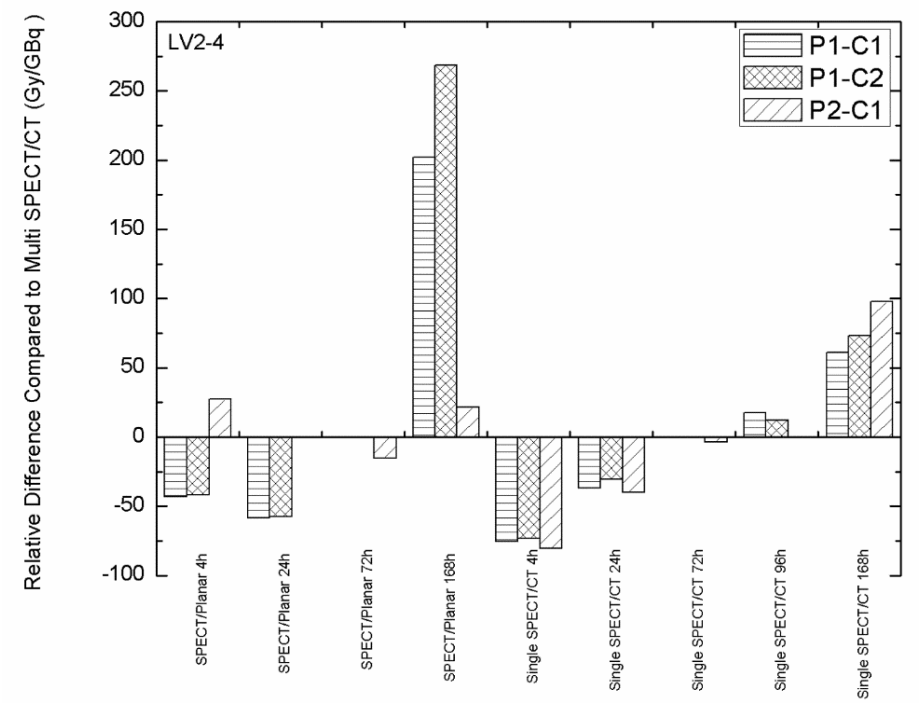

Figure 4.6. The relative difference in the calculated absorbed doses of lumbar vertebra 2-4 for the patients in each treatment cycle, taking reference the scanning mode 1

(P1-C1: patient 1- treatment cycle 1, P1-C2: patient 1- treatment cycle 2, P2-C1: patient 2- treatment cycle 1, Multi 3D: the scanning mode 1 including multiple 3D scans; SPECT/Planar 4 h: the scanning mode 2 including multiple planar scans in combination of one abdomen 3D scan at 4 h post-injection, SPECT/Planar 24 h: the scanning mode 2 including multiple planar scans in combination of one abdomen 3D scan at 24 h post-injection, SPECT/Planar 72 h: the scanning mode 2 including multiple planar scans in combination of one abdomen 3D scan at 72 h post-injection, SPECT/Planar 168 h: the scanning mode 2 including multiple planar scans in combination of one abdomen 3D scan at 168 h post-injection; Single 3D 4 h: the scanning mode 3 including one 3D scan at 4 h, Single 3D 24 h: the scanning mode 3 including one 3D scan at 24 h, Single 3D 72 h: the scanning mode 3 including one 3D scan at 72 h, Single 3D 96h: the scanning mode 3 including one 3D scan at 96h, Single 3D 168 h: the scanning mode 3 including one 3D scan at 168 h.)

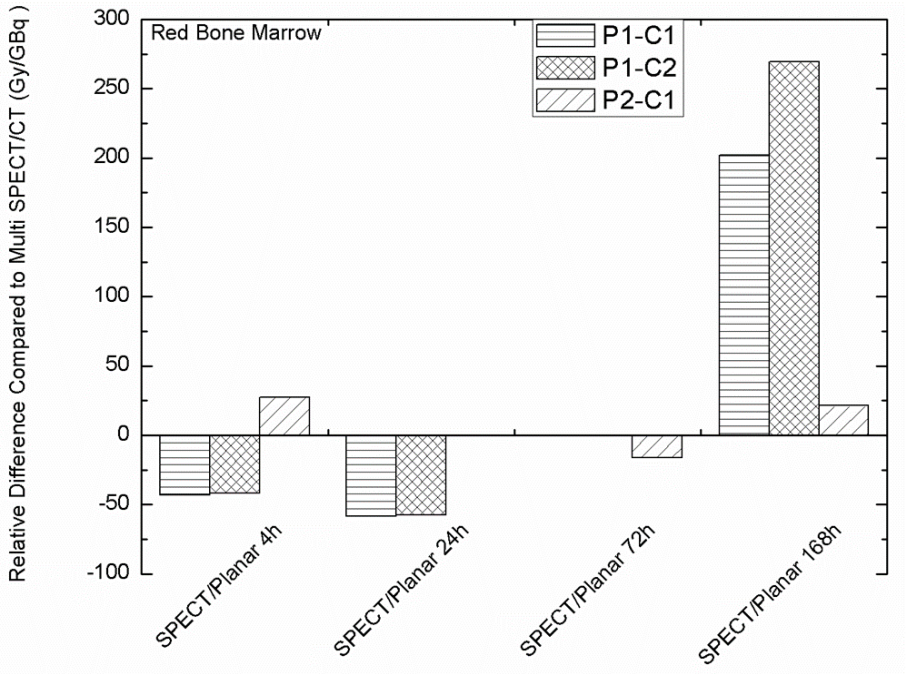

Figure 4.7. The relative difference in the calculated absorbed doses of the red bone marrow for the patients in each treatment cycle, taking reference the scanning mode 1 (P1-C1: patient 1- treatment cycle 1, P1-C2: patient 1- treatment cycle 2, P2-C1: patient 2- treatment cycle 1, Multi 3D: the scanning mode 1 including multiple 3D scans, SPECT/Planar 4 h: the scanning mode 2 including multiple planar scans in combination of one abdomen 3D scan at 4 h post-injection, SPECT/Planar 24 h: the scanning mode 2 including multiple planar scans in combination of one abdomen 3D scan at 24 h post-injection, SPECT/Planar 72 h: the scanning mode 2 including multiple planar scans in combination of one abdomen 3D scan at 72 h post-injection, SPECT/Planar 168 h: the scanning mode 2 including multiple planar scans in combination of one abdomen 3D scan at 168 h post-injection)

5. DISCUSSION

In this study, two metastatic prostate cancer patients who received ^{177}Lu[Lu]-PSMA-617 treatment were included with the intention of studying image-based red bone marrow dosimetry.

The main limitation of the study is the number of patients. Generally, ^{177}Lu[Lu]-PSMA-617 treatment is given to patients with bone and spine metastases. When red bone marrow dosimetry is performed, tumors in or near the segmented area may result in an over or underestimation of the absorbed dose. In order not to cause any under or over estimations due to tumors in or around the analysed area, we included in our study those patients who did not have tumors in the lumbar vertebrae and surrounding areas.

It was difficult to find patients who meet this criterion since these patients are transferred from the oncology departments to the nuclear medicine departments at the stage when there are extensive bone metastases. In addition, the pandemic has made the situation even more difficult since we started collecting the patient data when the pandemic was at its most intense stage. Another problem related to finding the patients is health insurance, since health insurance in Turkey does not cover the PSMA labelled treatments. Further limitations were related to clinical routine.

Performing and collecting the data for the WB planar and 3D scans for multiple time-points (e.g., more than four times) post-injection, particularly for late time-points (e.g., >140 h post-injection), could be very demanding. Although the scanning mode 1 provides the most accurate results, it requires long scan duration and this is not practical for the technicians and the patients as well. Although the scanning mode 2 requires a less acquisition duration, it mainly causes over- or underestimations in absorbed dose calculations associated with organ-count overlays. Although the number of organ-count overlays was minimized in our study (because the LV2-4 region had no visible 2D organ-count overlays), we observed underestimated and overestimations in the calculated absorbed doses compared to the imaging-protocol 1 based results. The calculated underestimations and overestimations might be highly related to the inhomogeneous background contributions during the time period.

There is also another limitation in our study which is related to our camera system memory. The CT scan at 96 h post-injection for patient 1 and the CT scan at 24 h post-injection for patient 2 was not available. In the segmentation program, which is under research, the loaded SPECT and CT scans must be the same study date. Therefore, for the

scanning mode 2 analysis, we needed to exclude the corresponding data set. Nevertheless we could find a solution for that issue for the investigations of the scanning mode 1 and 3, our segmentation program allowed us to use the CT data of the same patients, which were acquired at different day. With this solution, the required measurements for the scanning modes 1 and 3 could be done.

For the most preferred approach in the literature, the scanning mode 2, including the 3D scan at 24 h post-injection, showed the max relative difference as -59% and the min relative difference as -15% in the absorbed doses of the red bone marrow compared to the results based on the scanning mode 1.

The following can be used to explain this:

1) For WB planar scans, there is no accurate attenuation correction method. In our investigation, attenuation on the patients' WB planar scans, which would still underestimate or overestimate the number of counts compared to the 3D scans, was corrected using the geometric mean.

2) In WB planar and 3D scans, an inhomogeneous and time-varying background contribution occurs, particularly due to the presence of overlapping organs. This impact may be primarily responsible for the calculated high difference between the absorbed doses per injected activity values compared to the scanning mode 1. The absorbed doses could be overestimated or underestimated depending on how inhomogeneous the background contributions are and how they evolve over time.

Compared to the scanning mode 1, the highest relative difference in the red bone marrow was calculated for the scanning mode 2, including a 3D scan at 168 h post-injection (the maximum relative difference: 269%). It is highly associated with the low count statistic obtained at 168 h scan time point.

The lowest relative differences in the red bone marrow absorbed doses were calculated between the scanning mode 1 and the scanning mode 3, including the 3D scan at 72-96 h post injection (the range of the relative difference: -4% –+18%). The scanning mode 3 did not only provide similar results compared to the results based on the scanning mode 1, but also required the shortest acquisition duration compared to the scanning modes 1 and 2. Therefore, it is practical and it does not require the patients to come to the hospital more than once to have the imaging procedure repeated, so it is very comfortable for the patients as well as the technicians.

Nevertheless, it is important to keep in mind that there is a condition to apply this protocol. When this condition is not taken into account, it might not result in similar absorbed doses compared to the results based on the scanning mode 1. The ratio of t_{scan}/T_{eff} (t_{scan}: scan time, T_{eff}: effective half-life) should be in the range of 0.75 - 2.5. The t_{scan}/T_{eff} ratio was 0.04, 0.21, 0.64, 0.85, and 1.49 for the scanning mode 3, including the 3D scan at 4, 24, 72, 96, and 168 h, respectively.

Based on our calculations, the results based on the scanning mode 3, including a 3D scan at 72 h post-injection were very similar to the scanning mode 1 (the relative difference compared to the scanning mode 1: -4%), although the t_{scan}/T_{eff} ratio was slightly out of the determined (t_1/Teff for the scanning mode 3 including 72 h 3D scan: 0.64). It should be noted that unlike our study which was performed with ^{177}Lu[Lu]-PSMA-617, the study in where this range was determined was performed with ^{177}Lu[Lu]-DOTATATE. The main reason that we found similar absorbed doses compared to the scanning mode 1 based result although the t_{scan}/T_{eff} ratio was slightly out of the range could be associated with using the different pharmaceuticals. The single time point 3D based dosimetry (the scanning mode 3 based dosimetry) is quite new technique and the required exact scan time point post-injection is not standardized for each radiopharmaceutical yet, therefore, several investigations and implementations needs to done including more patient data as well as with considering different radiopharmaceuticals.

Literature Comparison:

Svensson et al. and Hagmarker et al. performed the red bone marrow dosimetry for the [^{177}Lu]Lu-DOTATATE administered patients by using multiple planar scans at 2, 24, 48, and 168 h post-injection in combination with one 3D scan at 24 h post-injection. The same scanning mode was investigated in our study as the scanning mode 2, including the 3D scan at 24 h post-injection. In the study by Svensson et al., lumbar vertebra 4 based region drawing was used for the dosimetry of red bone marrow of 46 patients with advanced neuroendocrine tumours, whereas in the study by Hagmarker et al., the segmentations for the lumbar vertebra 4, the lumbar vertebra 1-5, the thoracic vertebrae 1-12, and all visible vertebrae were used for the red bone marrow. Similarly, we segment the lumbar vertebrae 2-4 region for the red bone marrow dosimetry.

In the study of Svensson et al., the mean absorbed dose to the bone marrow, which was determined based on the lumbar vertebra 4 by using multiple planar scans in combination with one 3D scan at 24 h post-injection, was reported as 0.20±0.05

Gy/7.4GBq. In our study, the mean absorbed dose of the red bone marrow based on the lumbar vertebrae 2-4 by using multiple planar scans in combination with one 3D scan at 24 h post-injection was 0.13 Gy/7.4GBq. The relative difference in the mean absorbed doses of the red bone marrow between our study and the study by Svensson et al. was -35%.

In the study of Hagmarker et al., the reported median absorbed doses of the red bone marrow based on the segments of the lumbar vertebra 4 and the lumbar vertebrae 1–5 were 0.36 Gy/7.4GBq and 0.39 Gy/7.4GBq, respectively.

In our study, the median absorbed dose of the scanning mode 2, including the 3D scan at 24 h post-injection to the bone marrow determined from the lumbar vertebrae 2-4, was 0.13 Gy/7.4GBq.

The relative difference in the median absorbed doses of the red bone marrow between our results and the study of Hagmarker et al. based on the segments of the lumbar vertebra 4 and the lumbar vertebrae 1–5 was -64% and -67%, respectively.

The reason for the calculated differences in the absorbed doses between our study and the studies by Svensson et al. and Hagmarker et al. is probably related to the use of different radiopharmaceuticals. Another difference between our study and the study of Hagmarker et al. that may affect the results of absorbed doses was that they drew small spherical 3D segments on the vertebrae.

Patients with metastatic castration-resistant prostate cancer treated with ^{177}Lu[Lu]-PSMA-617 were investigated in the study by John Violet et al. The dosimetry was performed based on multiple 3D scans at 4, 24, and 96 h after injection. A 3D segmented complete skeleton region was drawn for the red bone marrow dosimetry.

In the study by John Violet et al., the range of the absorbed dose per administered activity of the red bone marrow was reported as 0.074–2.52 Gy/7.4GBq, and the mean absorbed dose per administered activity of the red bone marrow was 0.814 Gy/7.4GBq.

In our study, the mean absorbed dose of the red bone marrow for the scanning mode 1 (multiple 3D method similar to the imaging method used in the study by John Violet et al.) was calculated based on the segments drawn on the lumbar vertebrae 2-4, as 0.33 Gy/7.4GBq and the range is 0.22-0.39 Gy/7.4GBq.

In this study, the mean absorbed dose for the red bone marrow using the scanning mode 1 was 0.332 Gy/7.4GBq with the relative difference of -59% to the result in the study by Violet et al. since the result in this study was 0.814 Gy/7.4GBq.

The main factor for the differences in results may be that our patients had extensive bone metastases and spinal metastases, unlike our patients.

Table 5.1. Absorbed doses of the scanning modes 1, 2, 3 and relative differences of the scanning modes 2 and 3 compared to the scanning mode 1

Method	**Absorbed Dose (Gy/7.4GBq)**	**Relative difference compared to scanning mode 1 (%)**
Scanning mode 1 (Multi 3D method)	0.22-0.39	–
Multi Planar plus one 3D method 4 h	0.13-0.49	-43 – +27
Multi Planar plus one 3D method 24 h	0.09-0.16	-59 – -57
Multi Planar plus one 3D method 72 h	0.33	-15
Multi Planar plus one 3D method 168 h	0.47-1.42	+21 – +269
Single SPECT Method 4 h	0.07-0.13	-81 – -73
Single SPECT Method 24 h	0.18-0.33	-40 – -31
Single SPECT Method 72 h	0.49	-4
Single SPECT Method 96h	0.33-0.53	+12 – +18
Single SPECT Method 168 h	0.45-1.00	+61 – +98

In addition, there is one preclinical study by Beykan et al. in which the same three scanning modes were tested. In the study by Beykan et al., the kidney dosimetry for ^{177}[Lu]Lu-OPS administered pigs and a 3D printed phantom was investigated by using 3 different scanning modes (similar to our study) (1). Similarly, compared to the absorbed doses based on the multiple 3D scans, they found that the most similar absorbed doses were calculated by performing a single 3D based imaging at approximately 100 h post-injection. In addition, they reported underestimations of 34% for the multiple planar in the combination of a 3D scan based dosimetry, which is again a similar case in our study.

6. CONCLUSION

In this study, image based red bone marrow dosimetry was performed on metastatic prostate cancer patients treated with [^{177}Lu]Lu-PSMA-617 using three different scanning modes.

Although multiple 3D imaging is the most accurate scanning mode, the results of this study showed that it requires a lot of time and it is challenging to implement into clinical practice. The most common scanning mode used for the ^{177}Lu dosimetry in the literature includes multiple planar scans in combination of one 3D at 24 h post-injection. This method resulted in approximately 60% underestimations in the absorbed doses compared to multiple 3D dosimetry (related to the lack of reliable 2D background subtraction and 2D attenuation correction).

Based on our study, the best alternative imaging approach for the [^{177}Lu]Lu-PSMA-617 dosimetry instead of multiple 3D imaging based dosimetry could be performing the dosimetry based on a single 3D imaging at 72/96 h post-injection. Based on our comparisons between multiple 3D based dosimetry and single 3D based dosimetry at 72/96 h post-injection, the calculated minimum and maximum relative difference for the absorbed doses of the lumbar vertebrae 2-4 was -4% and 18%, respectively. However, it is significant to note that our results were based on a very small number of patient data and a single time-point 3D dosimetry needs comprehensive information about the biokinetics of the radiopharmaceutical used as well as the ideal scan time after the injection of the radiopharmaceutical. In addition, the region or organ to be analysed must be carefully selected in order to perform a single time-point 3D dosimetry.

7. REFERENCES

1. Beykan S. and Tran-Gia J. Is a single late SPECT/CT based kidney ^{177}Lu dosimetry superior to hybrid dosimetry with sequential multiple time-point whole-body planar scans in combination with an early SPECT/CT? *Physica Medica* 100 (2022) 39–50
2. Konijnenberg M, Herrmann K, Kobe C, et al. EANM position paper on article 56 of the Council Directive 2013/59/Euratom (basic safety standards) for nuclear medicine therapy. *Eur J Nucl Med Mol Imaging* 2021;48:67-72.
3. Kwekkeboom D.J., de Herder W.W., Kam B.L., et al. Treatment With the Radiolabeled Somatostatin Analog [^{177}Lu-DOTA0,Tyr3]Octreotate: Toxicity, Efficacy, and Survival. *J Clin Oncol* 2008;26:2124-2130.
4. Kwekkeboom D.J., Bakker W.H., Kooij P.P.M., et al. [^{177}Lu-DOTA0,Tyr3]octreotate: comparison with [111In-DTPA0]octreotide in patients. *Eur J Nucl Med* (2001) 28:1319–1325
5. Svensson J., and Rydén T., A novel planar image-based method for bone marrow dosimetry in ^{177}Lu-DOTATATE treatment correlates with haematological toxicity. *EJNMMI Physics* (2016) 3:21
6. Hagmarker L, Svensson J, Ryden T, et al. Bone marrow absorbed doses and correlations with hematological response during ^{177}Lu-DOTATATE treatments are influenced by image-based dosimetry method and presence of skeletal metastases. *J Nucl Med* 2019. 60:1406–1413
7. Violet J., Jackson P., Ferdinandus J., et al. Dosimetry of ^{177}Lu-PSMA-617 in Metastatic Castration-Resistant Prostate Cancer: Correlations Between Pretherapeutic Imaging and Whole-Body Tumor Dosimetry with Treatment Outcomes. *J Nucl Med* 2019; 60:517–523
8. Cherry S.R., Sorenson J.A., Phelps M.E. Physics in Nuclear Medicine 3rd ed. Philadelphia, PA: Saunders ; 2012
9. A. G. Webb Introduction to Biomedical Imaging 1st ed. Urbana IL: Wiley; 2017
10. Andreou M.M., Georgantzoglou A., Kordolaimi S., Lagopati N., Ploussi A., Salvara A.-L. and Vamvakas I. Nuclear Medicine Therapy Radioisotopes Production and Dosimetry. *Curr. Med. Imaging Rev*., 2013,9,51-75
11. Pacak K., ¬Taïeb D., ed. Diagnostic and Therapeutic Nuclear Medicine for Neuroendocrine Tumors. Springer: Switzerland; 2017

12. Dash A., Pillai M.R.A., Knapp Jr. F. F. Production of ^{177}Lu for Targeted Radionuclide Therapy: Available Options. *Nucl Med Mol Imaging* (2015) 49:85–107
13. Israel O., Pellet O., Biassoni L., et al. Two decades of SPECT/CT – the coming of age of a technology: An updated review of literature evidence. *Eur J Nucl Med Mol Imaging*. 2019; 46:1990–2012
14. Beykan S. Implementation and Optimization of Dosimetry for Theranostics in Radiopeptide Therapies Würzburg, Julius-Maximilians-Universität Würzburg, 2019
15. Bushberg J. T., Seibert J.A., Leidholdt Jr E.M., Boone J.M. The Essential Physics of Medical Imaging. Lippincott Williams & Wilkins: Philadelphia, PA; 2001
16. Ljungberg M. and Gleisner K.S. 3-D Image-Based Dosimetry in Radionuclide Therapy. IEEE trans. radiat. plasma med. sci. vol. 2, no. 6, 527-540
17. Madsen M.T. Computer Acquisition of Nuclear Medicine Images
18. Quantitative Nuclear Medicine Imaging: Concepts, Requirements and Methods IAEA Human Health Reports No. 9: Austria; 2014
19. Ljungberg M., Celler A., Konijnenberg M.W., Eckerman K.F., Dewaraja Y.K. and Sjögreen-Gleisner K. MIRD Pamphlet No. 26: Joint EANM/MIRD Guidelines for Quantitative ^{177}Lu SPECT Applied for Dosimetry of Radiopharmaceutical Therapy. *J Nucl Med.* 2016; 57:151–162
20. Thielemans K., Tsoumpas C., Mustafovic S., Beisel T. STIR: software for tomographic image reconstruction release 2. *Phys. Med. Biol* 2012
21. Ljungberg M. and Pretorius H. SPECT/CT: an update on technological developments and clinical applications. *Br J Radiol.* 2016;
22. Hennrich U. and Eder M. [^{68}Ga]Ga-PSMA-11: The First FDA-Approved 68Ga-Radiopharmaceutical for PET Imaging of Prostate Cancer. *Pharmaceuticals*. 2021; 14, 713.
23. Nanabala R., Sasikumar A., Joy A. and Pillai MRA. Preparation of [^{177}Lu]PSMA-617 Using Carrier Added (CA) ^{177}Lu for Radionuclide Therapy of Prostate Cancer. *J Nucl Med Radiat Ther*. 2016; 7:5
24. Fakiri M.E., Geis N.M, Ayada N., Eder M. and Eder A. PSMA-Targeting Radiopharmaceuticals for Prostate Cancer Therapy: Recent Developments and Future Perspectives. *Cancers* 2021, 13, 3967.

25. Chen J., Qi1 L., Tang Y. et al. Current role of prostate-specific membrane antigen-based imaging and radioligand therapy in castration-resistant prostate cancer. *Cell Dev. Biol*. 2022 10:958180.
26. Fanti S., Briganti A., Emmett L., et al. EAU-EANM Consensus Statements on the Role of Prostate-specific Membrane Antigen Positron Emission Tomography/Computed Tomography in Patients with Prostate Cancer and with Respect to [^{177}Lu]Lu-PSMA Radioligand Therapy. *Eur Urol Oncol* (2022)
27. Rosar F., Hau F., Bartholomä M., et al. Molecular imaging and biochemical response assessment after a single cycle of [^{225}Ac]Ac-PSMA-617/[^{177}Lu]Lu-PSMA-617 tandem therapy in mCRPC patients who have progressed on [^{177}Lu]Lu-PSMA-617 monotherapy. *Theranostics*, 2021; 11(9): 4050-4060
28. Hindorf C., Glatting G., Chiesa C., Lindén O., Flux G. EANM Dosimetry Committee guidelines for bone marrow and whole-body dosimetry. *Eur J Nucl Med Mol Imaging*, 2010
29. Traino A.C., Ferrari M., Cremonesi M. and Stabin M.G. Influence of total-body mass on the scaling of S-factors for patient-specific, blood-based red-marrow dosimetry. *Phys. Med. Biol*. 2007; 5231–5248
30. Beykan S., Dam J.S., Eberlein U., et al. ^{177}Lu-OPS201 targeting somatostatin receptors: in vivo biodistribution and dosimetry in a pig model. *EJNMMI Res*. 2016;6(1).
31. Forrer F., Krenning E.P., Kooij P.P., et al. Bone marrow dosimetry in peptide receptor radionuclide therapy with [^{177}Lu-DOTA0,Tyr3]octreotate. *Eur J Nucl Med Mol Imaging*. 2009; 36:1138–1146
32. Lassmann M, Eberlein U. Radiation Dosimetry Aspects of ^{177}Lu. Curr *Radiopharm.* 2015;8:139-144
33. Andersson M., Johansson L., Eckerman K. and Mattsson S. IDAC-Dose 2.1, an internal dosimetry program for diagnostic nuclear medicine based on the ICRP adult reference voxel phantoms. *EJNMMI Research*. 2017
34. Stabin M. Nuclear medicine dosimetry. *Phys. Med. Biol.* 51; 2006 R187–R202
35. Kletting P., Maas C., Kull. T., et al. Optimized peptide amount and activity for Y-90-labeled DOTATATE therapy. *J Nucl Med.* 2016; 57:503–508
36. Hänscheid H., Lapa C., Buck A.K., Lassmann M., Werner R.A. Dose mapping after endoradiotherapy with ^{177}Lu-DOTATATE/DOTATOC by a single measurement after 4 days. *J Nucl Med* 2018;59:75–81.

APPENDIX A: CV

Özgeçmiş

Kişisel Bilgiler

Adı	BERFU	**Soyadı**	NACAR

Öğrenim Durumu

Derece	Alan	Mezun Olduğu Kurumun Adı	Mezuniyet Yılı
Doktora			
Yüksek Lisans			
Lisans	Fizik	**Yeditepe Üniversitesi**	2019
Lise		**Adana Gündoğdu Koleji**	2013

Başarılmış birden fazla sınav varsa(KPDS, ÜDS, TOEFL; EELTS vs), tüm sonuçlar yazılmalıdır

Bildiği Yabancı Dilleri	Yabancı Dil Sınav Notu (**#**)

İş Deneyimi (Sondan geçmişe doğru sıralayın)

Görevi	Kurum	Süre (Yıl - Yıl)
		-
		-

Bilgisayar Bilgisi

Program	Kullanma becerisi

*****Çok iyi, iyi, orta, zayıf olarak değerlendirin

Bilimsel Çalışmaları

SCI, SSCI, AHCI indekslerine giren dergilerde yayınlanan makaleler

Diğer dergilerde yayınlanan makaleler

Uluslararası bilimsel toplantılarda sunulan ve bildiri kitabında (*Proceedings*) basılan bildiriler

Hakemli konferans/sempozyumların bildiri kitaplarında yer alan yayınlar

Diğer (Görev Aldığı Projeler/Sertifikaları/Ödülleri)
